Instituto de Geociências
Programa de Pós-Graduação em Geociências

UNIVERSIDADE FEDERAL DO RIO GRANDE DO SUL
INSTITUTO DE GEOCIÊNCIAS
PROGRAMA DE PÓS-GRADUAÇÃO EM GEOCIÊNCIAS

UM ESTUDO SOBRE MODELAGEM DE ONDAS OCEÂNICAS NO ATLÂNTICO SUDOESTE E UMA REPRESENTAÇÃO ESPAÇO-TEMPORAL UNIFORME DE DADOS DE SATÉLITE.

HEITOR PEROTTO

ORIENTADOR - Prof. Dr. Leandro Farina

Volume I

Porto Alegre - Novembro de 2017

Programa de Pós-Graduação em Geociências - UFRGS
Av. Bento Gonçalves 9500 - Agronomia - Cx. P. 15.001 - Prédio 43.113 S-207 - 91501-970 - Porto Alegre - RS
Tel.: (51) 3308-6340
E-mail: ppggeo@ufrgs.br

UNIVERSIDADE FEDERAL DO RIO GRANDE DO SUL
INSTITUTO DE GEOCIÊNCIAS
PROGRAMA DE PÓS-GRADUAÇÃO EM GEOCIÊNCIAS

UM ESTUDO SOBRE MODELAGEM DE ONDAS OCEÂNICAS NO ATLÂNTICO SUDOESTE E UMA REPRESENTAÇÃO ESPAÇO-TEMPORAL UNIFORME DE DADOS DE SATÉLITE.

HEITOR PEROTTO

ORIENTADOR - Prof. Dr. Leandro Farina

BANCA EXAMINADORA

Prof. Dr. Eduardo Puhl - Instituto de Pesquisas Hidráulicas, Departamento de Hidromecânica e Hidrologia, Universidade Federal do Rio Grande do Sul

Prof[a]. Dr[a]. Rita de Cássia Marques Alves - Departamento Geodésia, Universidade Federal do Rio Grande do Sul

Prof. Dr. Antonio Fernando Härter Fetter Filho - Centro de Filosofia e Ciências Humanas, Departamento de Geociências, Universidade Federal de Santa Catarina

Tese de Doutorado apresentada como requisito parcial para a obtenção do Título de Doutor em Ciências.

Porto Alegre - Novembro de 2017

Resumo

Ondas oceânicas são perturbações ocasionadas na superfície dos oceanos e são uma das fontes energéticas mais importantes para a modelagem da geometria das costas em todo o mundo constituindo-se um fator de risco às obras costeiras e operações em mar aberto. Este trabalho utilizou dados do modelo WAVEWATCH III (WW3) entre 2001 a 2009 como ferramenta para a obtenção de aspectos importantes em uma determinada região do Atlântico Sul que é vulnerável ao impacto de eventos extremos, ocasionados por ciclones extratropicais. Pelo fato de serem os principais controladores de padrões climáticos, causarem extremas mudanças no tempo e das maiores alturas de ondas serem geradas em sua região de influência, estes fenômenos meteorológicos são de grande importância para o estudo de ondas oceânicas e suas ações em regiões costeiras assim como também é importante conhecer sua origem, formação e trajetória. Com os dados das componentes U e V do vento provenientes do modelo foram calculadas as trajetórias dos ciclones extratropicais baseados na vorticidade relativa de seu centro. Ao todo, 28 eventos foram analisados dentro deste período. Estas foram classificadas com base em suas trajetórias em três padrões, o Padrão III é o mais comum (41,4%), com uma maior incidência de eventos que aparecem em maio. Os maiores valores de altura máxima e média foram gerados no outono e inverno, com uma maior incidência também em maio. O evento de maio de 2001 apresentou a ocorrência simultânea de dois ciclones causando danos à linha de costa em várias cidades. Os valores de altura de onda e intensidade do vento deste evento se mostraram superiores aos demais. Dados do satélite ENVISAT, obtidos por um sensor ASAR, foram comparados com os dados do modelo WW3 para o ano de 2007. Para comparar os dados de satélite com os dados de modelo foram utilizados dois algorítimos para uma representação espaço-temporal mais realista possível. Utilizando parâmetros estatísticos como viés, e índice de espalhamento a altura de swell foi analisada. Os dados de satélite mostraram uma grande uniformidade espacial comparados com os dados do modelo. Subestimação da altura de swell pelo modelo nos trópicos e em regiões específicas são encontradas em altas latitudes. Com o intuito de verificar e comparar os parâmetros de comportamento de ondas próximas de regiões costeiras, foi realizado um estudo de 6 eventos, 3 localizados na região sul, e mais 3 no nordeste do Brasil entre 2002 e 2009, priorizando eventos onde o swell era dominante. Estes eventos foram selecionados com base no intervalo no qual o satélite (ENVISAT) mede o comprimento de onda para uma comparação mais realista. Dados do modelo WW3 e do satélite foram utilizados como condições de fronteira para o modelo SWAN. Para cada evento as duas simulações foram comparadas com base no tempo e espaço e também para pontos específicos localizados em águas rasas e profundas. Observou-se que houve uma excelente correlação, evidenciada pelo coeficiente de Pearson, entre as duas simulações nas duas regiões estudadas, principalmente na análise espacial e temporal. Em águas rasas e profundas maior correlação é observada no sul. Constatou-se também que o período de pico T_p para a simulação com dados do WW3, é subestimado em relação à simulação com dados do satélite em todos os eventos. Os resultados mostram que houve uma grande coerência entre as duas simulações com valores de coeficiente de Pearson acima de 0.8. Embora o T_p aponte maior disparidade entre as duas simulações, a tendência da série histórica provou ser consistente em ambos os dados simulados; com o WW3 e com o satélite.

Abstract

Ocean waves are caused disturbances on the surface of the oceans and they are one of the most important energy sources for modeling the geometry of the coasts around the world and constituting a hazard to coastal works and offshore operations. This study used the WAVEWATCH III (WW3) model data from 2001 to 2009 as a tool to obtain important aspects in a particular South Atlantic region that is vulnerable to the impact of extreme events caused by tropical cyclones. Because they are the main weather patterns drivers, causing extreme changes in weather and greater heights of waves being generated in its area of influence, these meteorological phenomena are of great importance for the study of ocean waves and their actions in coastal regions and it is also important to know your origin, development and trajetory. With wind components U and V from the model trajectories of extratropical cyclones were calculated based on relative vorticity from its center. Altogether, 28 events were analyzed within this period. These were classified based on their trajectories in three patterns, the pattern III is the most common (41.4%), with a higher incidence of events that appear in May. The highest maximum and average height values were generated in the fall and winter, with a higher incidence also in May. The event of May 2001 featured the simultaneous occurrence of two cyclones causing damage to the coastline in several cities. The wave height and wind speed values of the event were higher than the others. ENVISAT satellite data obtained by a ASAR sensor, were compared with the WW3 model data for the year 2007. To compare the satellite data with the model data two algorithms were used to provide a space-time representation as realistic as posssible. Using statistical parameters such as bias and scattering index the swell height was analyzed. Satellite data showed a great spatial uniformity compared with model data. Underestimation of swell height by the model in the tropics and at specific regions high latitudes are found. In order to verify and compare the wave behavior near coastal regions, a study of six events was conducted, three located in the southern region, and three more in northeastern Brazil between 2002 and 2009, prioritizing events where swell was dominant. For a more realistic comparison these events were selected based on the range in which the satellite (ENVISAT) measures the wavelength. WW3 model data and the satellite were used as boundary conditions for the SWAN model. The two simulations were compared based on time and space and also to specific points located in shallow and deep water, for each event. It was observed that there was an excellent correlation shown by the Pearson correlation coefficient between the two simulations studied in both regions, particularly in the temporal and spatial analysis. In shallow and deep water highest correlation is observed in the south. It was also found that the peak period T_p for simulation WW3 data is underestimated in relation to simulation with satellite data on all events. The results show that there was a great coherence between the two simulations with Pearson coefficient values above 0.8. Although T_p points out greater disparity between the two simulations, the trend of the series proved to be consistent in both simulated data.

Sumário

Lista de Figuras

Lista de Tabelas

1 Introdução

As ondas são, entre os fenômenos naturais, um dos mais conhecidos e estudados pelo homem. Ondas oceânicas são perturbações ocasionadas na superfície dos oceanos. As principais ondas de superfície são as ondas de gravidade cuja força restauradora é a gravidade, as quais são geradas pelo vento. As características destas ondas dependem da velocidade e duração (tempo) da ação do vento e pela extensão da superfície aquosa sobre a qual o vento está soprando. Estão intimamente associadas às variações dos regimes atmosféricos, possuindo grande variabilidade espacial e temporal (CUCHIARA et al., 2006). São as principais e mais constantes fonte de energia no oceano, exercendo um papel fundamental na formação de feições costeiras (TOZZI; CALLIARI, 2000). No oceano aberto podem propagar-se por enormes distâncias com a perda mínima de energia. Quando chegam próximas a costa, sofrem diversos processos físicos que envolvem estruturas de conservação, adição e remoção de energia da onda. Os processos que removem a energia são a dissipação por fricção com o fundo, percolação e atenuação por viscosidade. As ondas próximas do seu centro de geração são denominadas de vagas (*sea*) quando já se encontram afastadas do seu centro de geração são denominadas ondulações (*swell*). Atingem a costa do Rio Grande do Sul através do quadrante sudeste (SE) (MOTTA, 1967; STRAUCH, 1996; COLI, 2000). Elas possuem um período longo e altura e distância entre as cristas regulares. As vagas são ondas mais irregulares com período menor que as ondulações.

O conhecimento do clima de ondas no tempo e no espaço é necessário para resolver a dinâmica dos processos morfodinâmicos e também para a realização de obras costeiras, recuperação e reconstrução praial e operações em mar aberto. Dados de campo são escassos na costa brasileira. Alguns estudos do clima de ondas foram realizados para determinadas áreas do sul do Brasil. Estes estudos foram baseados em diversas fontes de dados que abrangem observações visuais (MOTTA, 1963; MELO; ALVES, 1993), medições de campo (MOTTA, 1963; STRAUCH, 1998) e por sensoriamento remoto (COLI, 1994, 2000). Dados coletados em campo podem apresentar muitas falhas devido à falta de energia, perda do equipamento, manutenção, entre outras. Assim uma alternativa é o uso de dados oceanográficos obtidos por satélites para extrair dados como altura, período e direção da onda.

As medições de satélites tem apresentado importância cada vez maior em oceanografia, sobretudo pela extensão das áreas cobertas, número de observações, sua repetibilidade e o número de variáveis medidas, embora a acurácia das medições não seja muito grande e elas não possam ser estendidas a profundidades maiores, restringindo-se à superfície dos oceanos. De qualquer maneira, com o desenvolvimento da tecnologia de sensoriamento remoto, essas restrições tendem a ser superadas, sobretudo no que diz respeito a precisão das medições. Os sensores aplicados em satélites de observação oceânica utilizam a radiação eletromagnética para coletar as informações da superfície da água. Estes sensores podem ser passivos ou ativos. Os sensores passivos apenas recebem as ondas que emanam naturalmente da superfície. Por outro lado os sensores ativos são aqueles que emitem ondas e medem um ou mais parâmetros da onda que são refletidos. Os sensores ativos operam na faixa de micro-ondas e são também chamados de radares. Por operarem na faixa de micro-ondas e emitirem ondas, os radares tem a capacidade de realizarem medições continuamente, sob qualquer condição meteorológica. Dentro dos sensores ativos, destacam-se o escaterômetro, o radar altimétrico e o radar de abertura sintética (SAR), que medem aspectos dinâmicos como elevação da superfície, velocidade e direção do vento, cobertura de gelo (e seus movimentos), altura de onda e o espectro. O radar de abertura sintética avançada (ASAR) é uma versão aprimorada do instrumento SAR e é o único sensor, até o momento, capaz de obter medições do espectro direcional de ondas com cobertura contínua e global, e consequentemente, permitir a caracterização completa de um estado de mar. As características orbitais dos satélites se limitam às observações feitas durante as passadas que realiza com intervalos horários a diários. Sendo assim, as desvantagens do uso destes dados está ligado ao intervalo de tempo entre as medições e na restrição destas medidas a regiões localizadas colinearmente à trajetória do satélite (COLI, 1994).

Devido à escassez de dados coletados in situ, além dos dados de satélite, podemos utilizar a modelagem numérica como ferramenta para obter parâmetros de ondas para seu estudo e também para o fornecimento de previsões numéricas. A previsão do estado do mar é essencial para o projeto de construções de proteção costeira, portos e canais de navegação (SCHNEGGENBURGER; GÜNTHER; ROSENTHAL, 2000) também são importantes para atividades offshore como exploração de petróleo e navegação. Os modelos de onda, no entanto, não são aplicados apenas em previsões (*forecasting*), mas também usados com dados pretéritos (*hindcasting*)para prever a propagação de ondas em eventos passados, que podem auxiliar nos estudos relacionados à erosão costeira e transporte de sedimentos, estimativa da energia, projetos de portos e estruturas costeiras e oceânicas como plataformas de exploração de petróleo e também na reconstituição de eventos extremos, como furacões ou tempestades.

A implementação de um modelo de ondas utilizando condições de contorno que melhor representem os fenômenos atmosféricos caracterizam-se como uma ferramenta de simulação

bastante importante para o estudo da física das ondas (CUCHIARA et al., 2006). Nos modelos de primeira geração a interação não-linear é desprezada ou, se parametrizada, pouco significativa, sendo representada de uma forma simples (World Meteorological Organization, 1998). Nos modelos de segunda geração, a interação não-linear é representada através de parametrizações ou tratada através de forma simplificada, o que impede o crescimento independente dos diversos componentes do espectro. Os modelos de segunda geração tem dificuldade na representação de mares complexos gerados por rápidas mudanças nos campos de vento (GROUP, 1988). A primeira tentativa de produzir um modelo de terceira geração foi baseado em um método computacional introduzido por Hasselmann e Hasselmann (1981). Um grupo internacional de vários pesquisadores se uniu para desenvolver conjuntamente um modelo de terceira geração, que poderia ser implementado operacionalmente em escalas global e regional. O grupo WAM (GROUP, 1988) desenvolveu o modelo WAM que apresentou grande sucesso, devido ao algoritmo DIA criado por Hasselmann e Hasselmann (1985) que forneceu uma solução aproximada das interações não-lineares com muito baixo custo computacional. Desde o advento do algoritmo DIA, outros modelos de terceira geração têm sido desenvolvidos de forma independente do grupo WAM. Uma variação do modelo WAM foi desenvolvida por Tolman (1991) denominado WAVEWATCH. As descrições dos processo físicos no WAM e no WAVEWATCH são similares. Booij, Holthuijsen e Ris (1997) desenvolveu um modelo de terceira geração para aplicação em águas rasas e bacias fechadas. Tolman e Chalikov (1996) apresentaram um modelo de ondas com novas formulações para a entrada de vento e os termos de fonte de dissipação, bem como inovações no regime de propagação numérica usado no WAM.

Este estudo visa utilizar os dados de modelos numéricos para acompanhar eventos extremos no Atlântico Sul, bem como comparar estes dados com os do satélite ENVISAT e no comportamento do clima de ondas através de análises estatísticas.

1.1 Objetivos

O objetivo geral deste trabalho é a comparação espacial e temporal dos dados obtidos do espectro direcional de ondas obtidos pelo satélite ENVISAT, pelo sensor ASAR, com os dados obtidos pelo modelo WAVEWATCH III.

Além desse objetivo geral, serão abordados os seguintes objetivos específicos:

- Calcular as trajetória de ciclones extratropicais no Atlântico Sul entre 2001-2009 utilizando dados do modelo WW3.
- Obter dados de altura de swell através do espectro direcional de ondas adquirido do ENVISAT, em uma malha regular.

- Obter um algoritmo espaço-temporal que organize os dados de maneira uniforme.
- Comparar os resultados de simulações nas regiões sul e nordeste do Brasil utilizando dados de satélite e modelo como entrada.

1.2 Estrutura da Tese

Esta tese de doutorado está composta em torno de artigos científicos de acordo com a Norma 103 do Programa de Pós-Graduação em Geociências da Universidade Federal do Rio Grande do Sul. Os artigos foram submetidos à publicação em periódicos. Sendo assim, o corpo principal da tese (que equivale as sessões de resultados e discussões) é apresentado em três artigos.

- O capítulo 1 apresenta uma introdução sobre o tema da tese e também seus objetivos.
- O capítulo 2 contém a descrição dos métodos utilizados para aquisição dos dados utilizados nesta tese.
- Os capítulos 3, 4 e 5 corresponde ao corpo principal da tese onde estão localizados os três artigos científicos.
- O capítulo 6 abrange as considerações finais e principais conclusões.

2 Materiais e métodos

2.1 Dados de Satélite

Os dados de altura significativa e velocidade do vento para o artigo 1 foram obtidos através do Globwave (http://globwave.ifremer.fr/). Este projeto é uma iniciativa de três anos financiado pela Agência Espacial Europeia (ESA), para atender às necessidades dos usuários de produtos de onda obtidas por satélite em todo o mundo. Os dados usados foram adquiridos por altímetro que é um instrumento ativo que emite pulsos na banda de radar. O princípio consiste em medir com precisão a altitude de um satélite, através de pulsos, e em seguida, a distância entre o satélite e a superfície do alvo. Ao calcular a diferença entre os dois, a "altura da superfície do mar"é obtida. Esta altura da superfície do mar e, em particular quaisquer variações, pode ser usado para deduzir uma vasta quantidade de informações sobre o oceano e seus movimentos. Com os sistemas tais como Doris e GPS, que medem a posição do satélite de forma extremamente precisa, a altura da superfície do mar pode ser calculada com uma precisão de apenas alguns centímetros. Altimetria também pode determinar a altura de onda e velocidade do vento sobre o oceano, bem como a altura da superfície de lagos e rios, informações sobre campo de gravidade da Terra, o gelo do mar e a calota de gelo presente na topografia.

Sensores altimétricos estiveram presentes nos satélites Seasat em 1978, Geosat 1985-1988, ERS-1 e 2, de 1991, Topex / Poseidon, de 1992, e Jason de 2001. Os dados do altímetro têm sido utilizados para produzir mapas de médias mensais de alturas de onda e a variabilidade da densidade de energia das ondas no tempo e no espaço. Estes dados também são utilizados com os programas de previsão de ondas, para aumentar a precisão das previsões de ondas.

Os dados de altura significativa de swell e período de pico de swell, para os artigos 2 e 3, foram obtidos através do espectro direcional de ondas adquiridos pelo sensor ASAR do satélite ENVISAT.

O satélite ENVISAT foi lançado em março de 2002 pela Agência Espacial Europeia com instrumentos que pudessem substituir os dados enviados pelo satélite ERS, seu antecessor. O principal objetivo do ENVISAT foi fornecer dados da atmosfera, do oceano, da terra e do gelo, visando o monitoramento do aquecimento global, do grau de contaminação atmosférica

e dos riscos de desastres naturais. O ENVISAT possui dez instrumentos a bordo, divididos entre sensores ópticos e sensores ativos, sendo seu principal sensor óptico o MERIS (Medium Resolution Imaging Spectrometer) e seu principal sensor ativo o ASAR. A missão do satélite ENVISAT terminou em 08 de abril de 2012, após a inesperada perda de contato com o satélite.

O sensor ASAR é uma versão aprimorada do instrumento SAR que já estava em operação a bordo dos satélites ERS-1 e ERS-2; o ASAR tem uma antena de 10 m de comprimento, e operava em 5 modos distintos: modo de imagem, modo de polarização alternada, modo de ampla faixa, modo de monitoramento global e modo de onda. Estes modos possuem resoluções variando de 25 km a 1 km, especialmente desenvolvidos para observar áreas continentais, áreas oceânicas e calotas polares. Opera na banda C da faixa de micro-ondas do espectro eletromagnético. Tal sistema ilumina a superfície da Terra e recebe o sinal retroespalhado por essa área, processando-o para sintetizar uma imagem de alta resolução espacial. Por operarem na faixa de micro-ondas e o radar fornecer sua própria fonte de iluminação tem a capacidade de realizarem medições continuamente, sob qualquer condição meteorológica.

O sensor ASAR, no modo de onda, gera um tamanho mínimo de pequenas imagens, denominadas "imagettes", da superfície do mar de 5 km $\times$ 5-10 km, semelhante ao ERS SAR, ao longo de 100 km da órbita do satélite. Essas pequenas imagens são processadas para derivar os espectros de ondas da superfície do mar e, consequentemente, o comprimento de onda, período, altura e direção das ondas do mar.

2.2 Modelo de geração e propagação de ondas

2.2.1 WAVEWATCH III

O modelo WAVEWATCH III é um modelo de terceira geração desenvolvido pela NOAA/NCEP. Este modelo resolve a equação do balanço de ação para a energia espectral em termos de número de onda k e direção de onda θ, espaço $\mathbf{x}$ e tempo t (TOLMAN, 1999). Admitindo-se a ausência de corrente podemos expressar a equação do balanço a equação do balanço para a energia espectral como

$$\frac{DE(k,\theta,\mathbf{x},t)}{Dt} = S(k,\theta,\mathbf{x},t) = S_{in} + S_{nl} + S_{ds}, \tag{2.1}$$

onde o lado esquerdo é a taxa de variação da densidade de energia dos componentes da onda que viaja com a velocidade de grupo. O lado direito representa os termos fonte para a equação do balanço energético devido a entrada de energia do vento (S_{in}), transferência de energia não-linear por interações entre as ondas (S_{nl}) e dissipação (S_{ds}). O pressuposto nesta equação é que a escala de espaço e tempo de ondas individuais são muito menores que as escala

correspondentes à variação do espectro, das profundidades e correntes, quando consideradas.

2.2.2 SWAN

SWAN é um modelo de ondas de terceira geração, desenvolvido na Delft University of Technology, para obtenção de estimativas realistas de parâmetros de ondas em áreas costeiras, lagos e estuários a partir de condições de vento, batimetria e correntes (BOOIJ; RIS; HOLTHUIJSEN, 1999; RIS; HOLTHUIJSEN; BOOIJ, 1999). No entanto, SWAN pode ser usado em qualquer escala relevante para ondas de gravidade na superfície gerada pelo vento. O modelo é baseado na equação do balanço de ação das ondas (2.1) porém com termos fonte modificados e também adicionais devido a interação com a batimetria tais como, o atrito no fundo e quebra induzida pelo fundo.

Referências Bibliográficas

BOOIJ, N.; HOLTHUIJSEN, L.; RIS, R. The "Swan"Wave Model for Shallow Water. In: *Coastal Engineering 1996*. New York, NY: American Society of Civil Engineers, 1997. p. 668–676. ISBN 978-0-7844-0242-9. ISSN 08938717. Disponível em: <http://ascelibrary.org/doi/10.1061/9780784402429.053>.

BOOIJ, N.; RIS, R. C.; HOLTHUIJSEN, L. H. A third-generation wave model for coastal regions: 1. Model description and validation. *Journal of Geophysical Research*, v. 104, n. C4, p. 7649, 1999. ISSN 0148-0227. Disponível em: <http://doi.wiley.com/10.1029/98JC02622>.

COLI, A. B. *Análise das alturas de onda ao longo do Rio Grande do Sul: dados históricos e altimétricos*. 58 p. Monografia (Graduação em Oceanologia) — Fundação Universidade Federal do Rio Grande, 1994.

COLI, A. B. *Estudo do Clima Ondulatório em Rio Grande*. 76 p. Mestrado em Engenharia Oceânica — Fundação Universidade Federal do Rio Grande, 2000.

CUCHIARA, D. C. et al. Modelagem Numérica do Comportamento das Ondas na Costa do Rio Grande do Sul. In: *II Seminário e Workshop em Engenharia Oceânica*. Rio Grande - RS: [s.n.], 2006. v. 15, p. 15.

GROUP, T. W. The WAM Model - A Third Generation Ocean Wave Prediction Model. *Journal of Physical Oceanography*, v. 18, n. 12, p. 1775–1810, dec 1988. ISSN 0022-3670. Disponível em: <http://journals.ametsoc.org/doi/abs/10.1175/1520-0485(1988)018<1775:TWMTGO>2.0.CO;2>.

HASSELMANN, S.; HASSELMANN, K. *A symmetrical method of computing the nonlinear transfer in a gravity wave spectrum*. [S.l.]: Wittenborn, 1981. (Hamburger geophysikalische Einzelschriften / A).

HASSELMANN, S.; HASSELMANN, K. Computations and Parameterizations of the Nonlinear Energy Transfer in a Gravity-Wave Spectrum. Part I: A New Method for Efficient Computations of the Exact Nonlinear Transfer Integral. *Journal of Physical Oceanography*, v. 15, n. 11, p. 1369–1377, nov 1985. ISSN 0022-3670. Disponível em: <http://journals.ametsoc.org/doi/abs/10.1175/1520-0485(1985)015<1369:CAPOTN>2.0.CO;2 http://journals.ametsoc.org/doi/abs/10.1175/1520-0485%281985%29015%3C1369%3ACAPOTN%3E2.0.CO%3B2>.

MELO, E.; ALVES, J. H. G. M. Nota sobre a chegada de ondulações longínquas à costa brasileira. In: *Anais do X Simpósio Brasileiro de Recursos Hídricos*. Gramado - RS: [s.n.], 1993. v. 5, p. 362–369.

MOTTA, V. F. *Relatório - análise e previsão de alturas de onda em Tramandaí*. Porto Alegre - RS, 1963. 30 p.

MOTTA, V. F. *Estudo em modelo reduzido para a regularização da embocadura Lagunar de Tramandaí*. Porto Alegre - RS, 1967.

RIS, R. C.; HOLTHUIJSEN, L. H.; BOOIJ, N. A third-generation wave model for coastal regions: 2. Verification. *Journal of Geophysical Research*, v. 104, n. C4, p. 7667, 1999. ISSN 0148-0227. Disponível em: <http://doi.wiley.com/10.1029/1998JC900123>.

SCHNEGGENBURGER, C.; GÜNTHER, H.; ROSENTHAL, W. Spectral wave modelling with non-linear dissipation: validation and applications in a coastal tidal environment. *Coastal Engineering*, v. 41, n. 1-3, p. 201–235, sep 2000. ISSN 03783839. Disponível em: <http://linkinghub.elsevier.com/retrieve/pii/S0378383900000338>.

STRAUCH, J. C. S. Estudo do clima ondulatório em Rio Grande. In: *Anais do XII Congresso Regional de Iniciação Científica e Tecnologia em Engenharia*. Curitiba - PR: [s.n.], 1996. p. 51.

STRAUCH, J. C. S. Um Ano de Monitoramento de Ondas em Rio Grande. In: *XI Semana Nacional de Oceanografia*. Rio Grande - RS: [s.n.], 1998.

TOLMAN, H. L. A Third-Generation Model for Wind Waves on Slowly Varying, Unsteady, and Inhomogeneous Depths and Currents. *Journal of Physical Oceanography*, v. 21, n. 6, p. 782–797, jun 1991. ISSN 0022-3670. Disponível em: <http://journals.ametsoc.org/doi/abs/10.1175/1520-0485(1991)021%3C0782%3AATGMFW%3E2.0.CO%3B2>.

TOLMAN, H. L. *User manual and system documentation of WAVEWATCH-III version 1.18*. Washington, DC, 1999. 110 p.

TOLMAN, H. L.; CHALIKOV, D. Source Terms in a Third-Generation Wind Wave Model. *Journal of Physical Oceanography*, v. 26, n. 11, p. 2497–2518, nov 1996. ISSN 0022-3670. Disponível em: <http://journals.ametsoc.org/doi/abs/10.1175/1520-0485%281996%29026%3C2497%3ASTIATG%3E2.0.CO%3B2>.

TOZZI, H. A. M.; CALLIARI, L. J. Morfodinâmica da Praia do Cassino, RS. *Pesquisas em Geociências*, v. 27, n. 1, p. 29–42, 2000.

World Meteorological Organization. *Guide to Wave Analysis and Forecasting*. 2nd. ed. [S.l.]: World Meteorological Organization, 1998. 170 p. ISBN 9263127026.

3 Tracking extratropical cyclones which cause extreme ocean wave events in the Southwestern Atlantic Ocean

Acompanhamento de ciclones extratropicais que causam eventos extremos no Oceano Atlântico Sudoeste

Heitor Perotto[1], Leandro Farina[2,3] and Elírio Ernestino Toldo Jr[4]

[1] *Instituto de Geociências, Universidade Federal do Rio Grande do Sul, Porto Alegre, Brazil*,

[2] *Instituto de Matemática e Estatística e Centro de Estudos de Geologia Costeira e Oceânica, CECO Universidade Federal do Rio Grande do Sul, Porto Alegre, Brazil*,

[3] *Basque Center for Applied Mathematics (BCAM), Bilbao, Basque Country, Spain*

[4] *Centro de Estudos de Geologia Costeira e Oceânica (CECO)*,

Instituto de Geociências, Universidade Federal do Rio Grande do Sul, Porto Alegre, RS, Brazil.

Abstract

Extratropical cyclones generate large influence on the dynamics of the ocean waves, intensifying and causing increased storm surges that cause anomalous high sea level rises. The variability of ocean waves during the occurrence of extratropical cyclones in eastern south Atlantic, between 2001 and 2009 is examined. From a third-generation model, data of significant wave height, direction and wind speed were used to calculate the trajectories of cyclones based on the relative vorticity from its center. Altogether, 28 events were analyzed within this period. These were classified based on their trajectories in three patterns. To characterize the atmospheric conditions that originated these events was used reanalysis data. The highest values of maximum and average height were generated in the fall and winter with a higher incidence in May an pattern III being the most common. In addition, the extreme event of May 2001, generated by two simultaneous extracyclones caused a storm surge was analyzed in detail.

Keywords: Ocean waves, extratropical cyclones, cyclone tracks, storm surge.

Resumo

Os ciclones extratropicais geram grande influência na dinâmica das ondas oceânicas, intensificando-as e causando aumento das marés meteorológicas que causam elevação anômala do nível do mar. A variabilidade das ondas oceânicas durante a ocorrência de ciclones extratropicais no Atlântico Sul Oriental, entre 2001 e 2009, é examinada. A partir de um modelo de terceira geração, dados de altura significativa, direção e velocidade do vento foram utilizados para calcular as trajetórias dos ciclones com base na vorticidade relativa do seu centro. No total, 28 eventos foram analisados nesse período. Estes foram classificados com base em suas trajetórias em três padrões. Para caracterizar as condições atmosféricas que originaram esses eventos foram utilizados dados de reanálise. Os valores mais altos de altura máxima e média foram gerados no outono e no inverno com maior incidência em maio, sendo o padrão III o mais comum. Além disso, o evento extremo de maio de 2001, gerado por dois ciclones extratropicais simultâneos que causou uma maré meteorológica foi analisado em detalhes.

Palavras-chave: Nível do mar, modelo de onda, trajetórias dos ciclones, marés meteorológicas.

3.1 Introduction

Extratropical cyclones produce surface winds and those in contact with the surface of the ocean transfer energy, through friction, generating waves. This transfer is limited by the speed and duration of wind and the extent of the aqueous surface over which the wind is blowing. Thus, strong winds acts on the track, parallel to the coast, which intensifies when a center of low pressure is acting in conjunction with a central high pressure water in the coastal zone stack, while the low pressure associated with the cyclonic rotation increases the level of the ocean.

Although, extensively studied in the northern hemisphere (HADLOCK; KREITZBERG, 1988; CATTO; SHAFFREY; HODGES, 2011; CHAMPION et al., 2011; BERNHARDT; DEGAETANO, 2012), there are fewer works on the behavior and characterization of extratropical cyclones in the southern hemisphere (SINCLAIR, 1994; SELUCHI, 1995; SINCLAIR, 1995), particularly in the south Atlantic.

An important aspect that has been attracting the attention of the scientific community recently is the classification of the extratropical cyclones in the South Atlantic. Gan e Rao (1991) analyzed 10 years of data (January 1979 - December 1988) where they observed two preferred cyclogenesis regions in South America: one near Uruguay´s coast (31.5 $^\circ$ S and 55 $^\circ$ W), associated with the baroclinic instability due to the presence of the Andes to another over the Gulf of San Matias, Argentina, (42.5 $^\circ$ S and 62.5 $^\circ$ W), related to the baroclinic instability of the

westerlies. Rocha, Sugahara e Silveira (2004) analyzed six extratropical cyclones formed near the western South Atlantic between April and September 1999. They used hindcast information from third-generation wave model, showing wave heights up to 5 m in some events close to he Brazilian coast. Comparison with satellite altimeter data showed a systematic underestimation by 0.5 m of the significant wave height.

Parise, Calliari e Krusche (2009) analyzed twenty-three intense events storm tides between June 2006 and July 2007 in Cassino Beach, Brazil. According with their analysis, these extreme events have been more frequent in autumn and winter, with 35% prevalence in each of these two seasons of the year, followed by spring (17%) and summer (13%). They noticed that the SW winds occurred in 70% of the cases and were essential for the occurrence of elevations above sea level. These events were classified into three trajectory patterns: 1) cyclogenesis south of Argentina with a eastward shift of trajectory between 47.5 ° S and 57.5 ° S, 2) cyclogenesis to the south of Uruguay with eastward trajectory shift between 35 ° S and 42.5 ° S, 3) cyclogenesis in south of Uruguay with to shift to southeast and trajectory between 35 ° S and 57.5 ° S.

Dragani et al. (2010) investigated a possible increase in wave heights generated by wind in the southeastern continental shelf of South America between 32 ° S and 40 ° S. Using in situ time series (1996-2006) and annual average significant wave heights obtained by the satellite TOPEX (1993-2001), located on the continental shelf and in the adjacent ocean, they observed an apparently positive trend. The authors also implemented a version of the wave model SWAN forced with surface winds from the NCEP / NCAR in a regional domain for the period 1971-2005 for their study. The annual quadratic mean wave heights simulated showed significant positive trends in most of the inner shelf and in the adjacent ocean. They concluded that the most significant increase was observed between the years 80 and 90.

Bitencourt et al. (2011) examined intense wind events at the southern Brazilian coast associated with extratropical cyclones using wind speed observed at nine meteorological stations. They found that the winds are strongly associated with extratropical cyclones only south of 28 ° S.

Using a wave model with wind data reanalysis from 1979 to 2008, Machado et al. (2010), studied the wave energy in deep water (100 m) in the South Atlantic. The results indicated there were 40 extreme events (with at least 6 m wave height) in that period. Some of these events led to the erosion of 62.96 m^3 / m and 1,8 m of elevation above sea level. They identified four synoptic generating patterns synoptic for these situations. Among the 40 events, 53.66% had a history of pattern II and 26.82% were related to pattern III, both representing 80% of the total.

Dragani et al. (2013) recently studied synoptic patterns associated with extreme wave conditions at the Rio de la Plata mouth using data series from 1996 to 2009. They identified 80

events with significant wave heights higher than 3.5 m in this period and selected 3 case studies which were classified according with three synoptic patterns. Nevertheless, the cyclones tracks that generated those patterns were not examined in details by the authors.

The event of May 2001 caused extensive damage to the coast of Santa Catarina where 11 counties were affected. Along with the coast of Santa Catarina, damages were reported on the coast of Paraná, São Paulo and Rio de Janeiro. On the beach of Matinhos, in the state of Paraná, waves destroyed 19 homes and displaced about 35 families. About 4.5 km of coastline were hit hard by the wave force, and in some places the waves reached a height of 5 m and the sea has advanced 150 m to urban areas. On the coast of São Paulo, the sea invaded several neighborhoods of the cities of Santos and São Vicente, where the tide reached 1.5 m, according to the civil defense. Avenues, canals and storm sewers were clogged with lots of sand and some low walls were damaged or knocked down. Throughout the state of Rio de Janeiro, at least 160 families were left homeless. According to the newspapers, waves of 4 m were observed invading the streets and leaving lots of sand (INNOCENTINI; OLIVEIRA; Cunha Prado, 2003).

In the present work, we used data from 2001 to 2009 to analyze oceanography variables such as average and maximum significant wave height and wind speed and direction in a particular region of the South Atlantic which is vulnerable to the impact of extreme ocean waves and storm surges. In effect, we selected three locations on the south coast of Brazil possessing urban settlements, activities and residences very close to the ocean and thus very sensitive to its variability. There, the socioeconomic influences of the ocean intense events are therefore critical.

The contents of the article are the following. In the next section, we describe the dataset we used and explain the criteria to identify the extratropical cyclones trajectories. The general results and data are presented and discussed in the section 3.3. Next, we describe and quantify by means of wave and wind variables, the singular event that took place in May 2001 which combined two simultaneous cyclones and generated several damages on the coast, particularly in the city of Garopaba. This analysis was performed using the SWAN model and compared with satellite data. We offer a conclusion of the article in section 3.4.

3.2 Data and methods

The data used were obtained by the processing of the model WAVEWATCH III (TOLMAN, 1999). These have been located at the site ftp://polar.ncep.noaa.gov/pub /history/waves. The period is from 2001 to 2009. This time interval has been chosen according with documentation of existing extreme events that occurred and affected mostly the state of Santa Catarina in Brazil. In table 1, all the events analyzed are listed.

The implementation of this model from which the data was extracted consider the entire globe as its domain with spatial resolution of $1^\circ \times 1.25^\circ$ in latitude and longitude, respectively. The time step employed is 3 hours. Different wind fields are used and combined to force the wave system. These are available in intervals of 3 hour and obtained from the Global Data Assimilation Scheme (GDAS).

In order to calculate the cyclones tracks that occurred in the period of our interest, we used the zonal and meridional wind fields provided through the WAVEWATCH III output file, but generated by GDAS. The tracks, or trajectories, have been defined as a sequence of positions $[x(t), y(t)]$, where t is counted from the first identification of the cyclone to its disappearance. This time interval considered for each particular event is the duration of the cyclone life (ROCHA; SUGAHARA; SILVEIRA, 2004). The trajectories were calculated with the sequence of relative vorticity ζ_{10}, at the cyclone center, using the maximum negative vorticity of the geostrophic wind by using the formula Eq.(3.1)

$$\zeta_{10} = \frac{\partial_{v_{10}}}{\partial_x} - \frac{\partial_{u_{10}}}{\partial_y}, \tag{3.1}$$

where u_{10} e v_{10} are, respectively, the zonal and meridional components of wind measured at 10 m height with x representing the east-west, and y, the north-south direction. In order to better characterize the trajectory of systems that generate extremes, a threshold of vorticity less or equal to $(\zeta_{10}) = -1,5 \times 10^{-5}\, s^{-1}$ has been employed.

The Database Reanalysis Project R-1 NCEP / NCAR (National Centers for Environmental Prediction) was used to characterize the atmospheric conditions that originated events, primarily from May 2001. The zonal and meridional wind components were used at the 10 m height and atmospheric pressure, at mean sea level. Both quantities had spatial resolution of $2.5^\circ \times 2.5^\circ$ and temporal resolution of 6 h (0000, 0600, 1200, 1800 UTC) (KALNAY et al., 1996).

3.3 Results and Discussion

We will focus on the analysis of the wave impacts at three places. Namely, the coastal cities of Rio Grande, Tramandaí and Garopaba. These locations were chosen because their socio-economical importance in southern Brazil and the wider impact to which they are subjected to by being near the field of action of extratropical cyclones. Their locations are represented in figures 1–3. In the next subsection we examine the events overall and in the subsection 3.3.2, a special attention is put on the singular event of May 2001.

3.3.1 General View

In the period studied, we identify 28 extreme events associated to 28 ciclogenetic situations, occurring from latitude 30 ° S to latitude 55 ° S. The cyclones tracks can be classified into the three patterns proposed by Machado et al. (2010):

- Pattern I: Cyclogenesis at southern coast of Argentina moving eastward and track limited between latitudes 47.5 ° S and 57.5 ° S (Fig.3.1).
- Pattern II: Cyclogenesis at the south coast of Uruguay moving eastward with track limited between latitudes 28 ° S and 43 ° S (Fig.3.2).
- Pattern III: Cyclogenesis at south coast of Uruguay moving to southeast and tack between latitudes 32 ° S and 57.5 ° S (Fig.3.3).

The events are listed in Table 3.1, with the abovementioned patterns. The third event, occurred in May 2001, comprises two cyclones, but it is counted as a single event.

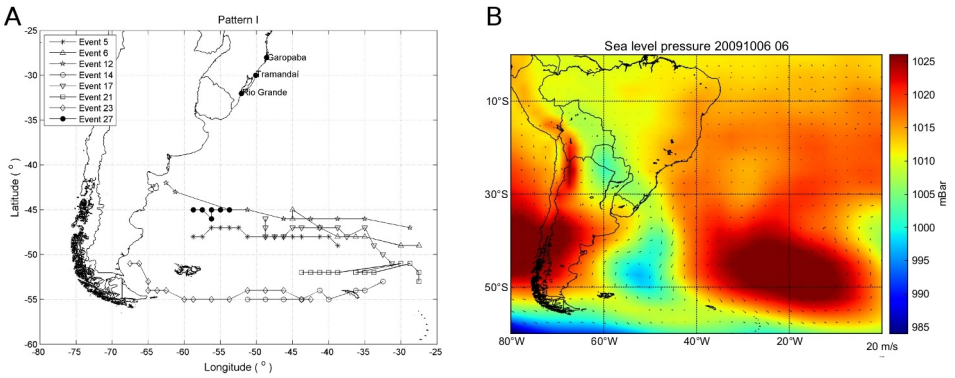

Figure 3.1: Cyclones tracks Pattern I (A) and synoptic situation (B).

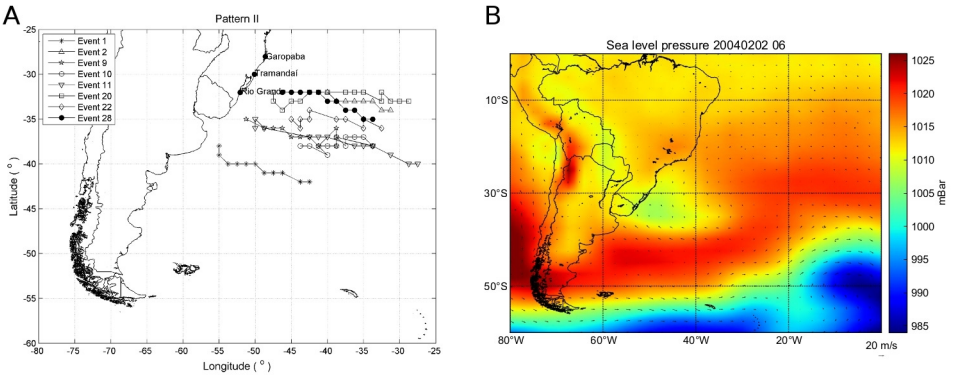

Figure 3.2: Cyclones tracks Pattern II (A) and synoptic situation (B).

Figures 3.1, 3.2 and 3.3 show the trajectories of cyclones addition, synoptic characteristics for patterns I, II and III respectively. In the pattern I the low pressure center is located between

Table 3.1: Events dates and their classification.

Events	Month	Year	Pattern
1	1	2001	II
2	2	2001	II
3	5	2001	Cyclone 1 II Cyclone 2 III
4	7	2001	III
5	10	2001	I
6	11	2001	I
7	2	2002	III
8	9	2002	III
9	5	2003	II
10	5	2003	II
11	2	2004	II
12	3	2004	I
13	5	2004	III
14	9	2004	I
15	5	2005	III
16	8	2005	III
17	6	2006	I
18	9	2006	III
19	7	2007	III
20	5	2008	II
21	6	2008	I
22	10	2008	II
23	11	2008	I
24	2	2009	III
25	4	2009	III
26	8	2009	III
27	10	2009	I
28	12	2009	II

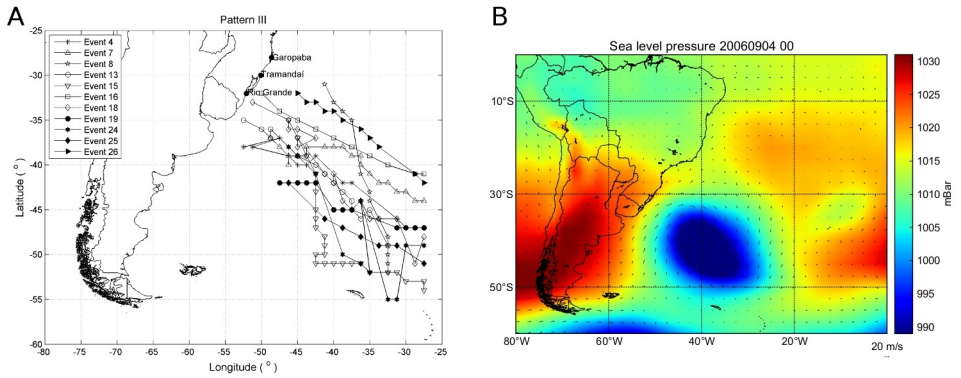

Figure 3.3: Cyclones tracks Pattern III (A) and synoptic situation (B).

two high pressure centers, one on the continent and another farther away in the open ocean. The presence of high pressure in the center of the continent contributes to the formation of a track with wind SW direction which contributes to the stacking of water in the coastal region by the effect of Ekmann. In pattern II the low pressure center is close to the shore causing the winds generated by Hurricane act directly on it. Consequently the cyclone remains longer near the coast and, therefore, the impact is more specific. And the pattern III the low pressure center moves to SE creating a trail toward SW wind.

The patterns III, II and I occur in 41.4%, 31% and 27.6% of the cases, respectively. We also observed that they occur more frequently in autumn (35.7%) and spring (25%) with 21.4% recorded in May alone. This higher frequency in autumn is associated with stronger winds from the south of Brazil at the time of the year (PARISE; CALLIARI; KRUSCHE, 2009). Figure 3.4 shows the prevailing winds in the three trajectory patterns for the three locations studied. For the pattern I the wind from NE prevailed in three locations, with the specific aspects that in Garopaba also occurred in the presence of N and S winds and Rio Grande, SE winds can be observed. In pattern II, winds from SW prevailed for three locations. In Garopaba, winds from N are also observed. In Tramandaí, winds from S and E and in Rio Grande, winds from S. For pattern III, wind from SW prevailed in Garopaba, W-SW in Tramandaí and S-SW in Rio Grande.

According to the figures of Table 3.2 we see that the highest values of average and maximum heights are associated with patterns II and III. The highest values of wind speed occurred in patterns II and III (Fig. 3.4). Parise, Calliari e Krusche (2009) analyzed 23 events for the Cassino Beach (RS) and noticed that the SW winds occurred in 70% of cases and were essential for the occurrence of elevations above sea level. Observing the wave height maximum and average values, we found that the larger values are associated with the patterns II and III (Table 3.2).

The higher values of average and maximum height were generated by events: 7, 10, 13, 14, 18, 19, 20 and 28. Among them, the events 10, 14, 18 and 28 showed very little variation between the average and maximum heights. The events with the largest wave heights occurred

more frequently in May, and in these events, pattern III occurs more frequently (50%). With respect to the wind velocity, the events 7, 10, 13, 15, 18, 19 and 20 produced the largest values of maximum and mean velocity. In these events, pattern III again occurs with highest frequency (42,9%).

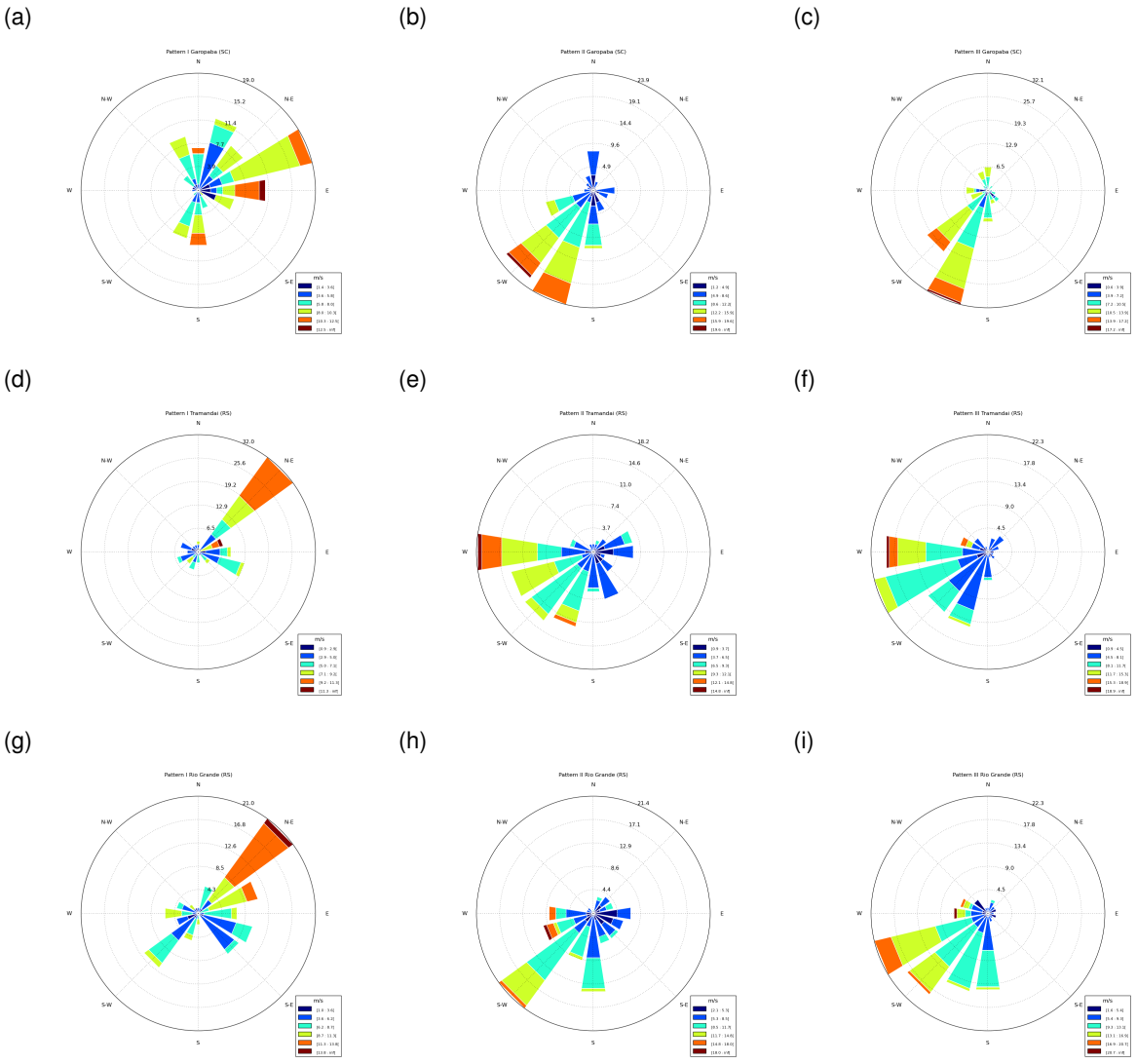

Figure 3.4: Wind direction and speed for the three patterns, on the studied locations.

Table 3.2: Mean and maxima wave heights.

	Pattern I	**Pattern II**	**Pattern III**
Mean Garopaba	2.19	2.77	2.77
Maximum Garopaba	3.73	5.36	5.01
Mean Tramandai	1.66	2.07	2.17
Maximum Tramandai	2.77	3.88	3.52
Mean Rio Grande	1.82	2.07	2.37
Maximum Rio Grande	2.92	3.76	3.78

Tozzi e Calliari (1999) described four major classes of storms to the coast of Rio Grande do Sul (Table 3.3). Storms furthest from mid-latitude 60 ° S and coastal events of East / Southeast

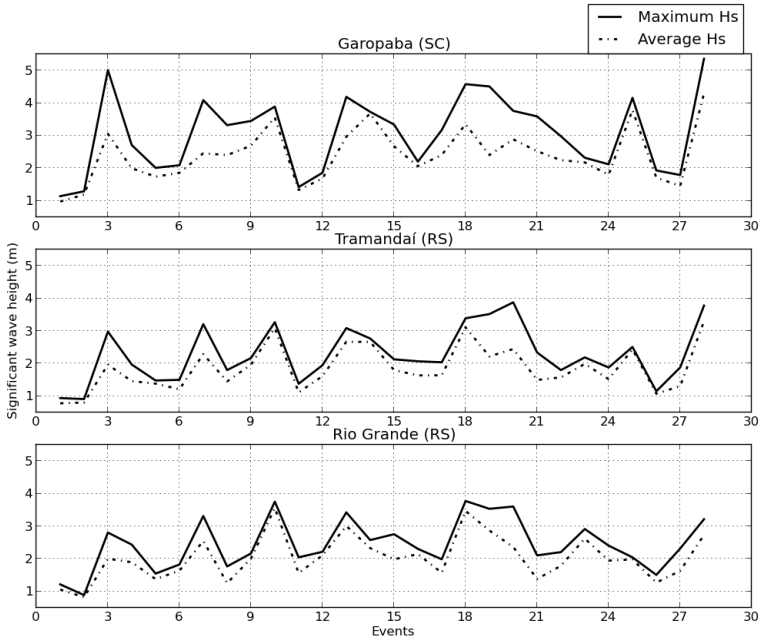

Figure 3.5: Significant wave height and average height for the three locations.

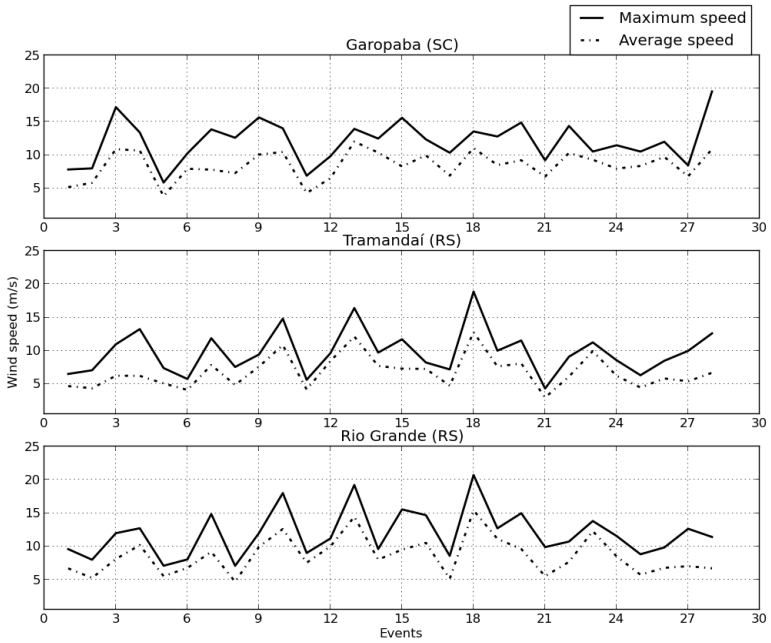

Figure 3.6: Maximum and average wind velocity for the three locations.

Table 3.3: Main characteristics of extratropical storms South Atlantic Ocean defined by Tozzi (1999). Source: Modified from Tozzi e Calliari (1999).

CHARACTERISTICS	STORMS			
	E/SE	S/SE	MIDDLE OF THE ATANTIC OCEAN	EXTRATROPICAL CYCLONES
Waves	0,5 - 1 m	1 - 1,5 m	>1,5 m	>2 m
High sea level elevation	<0,5 m	$\sim$ 1 m	>1 m	>1 m
Location	Far	Near	Along/Far	Near/Along
Subaerial volume	<10 m^3/m	10 a 20 m^3/m	20 a 50 m^3/m	50 a 80 m^3/m
Impact	Low	Moderate	Significant	Severe

predominate in the warm seasons. While the cold seasons, predominate near 30 $^\circ$ S storms, and coastal storms in the South / Southeast and storms of the middle of Atlantic Ocean.

According to the proposal by Tozzi e Calliari (1999) classification, the majority of events are classified as having a severe impact and high variation of sediment volume, in their area of influence, closer to shore. This classification agrres with the patterns of trajectories presented in this work.

3.3.2 Event of May 2001 (Event 3)

Because of its singular aspects, the third event, occurred in May 2001, will be described separately. This is associated with the simultaneous occurrence of two cyclones in most of the duration of the event. These cyclones which generated a severe storm surge that hit the coast of Santa Catarina. Elevated values of maximum and average significant wave height and wind velocity have been registered in the three locations, particularly in the region of Garopaba, as shown in Figure 3.5 and 3.6. Figure 3.8 shows the two tracks followed by the tropical cyclones, named here as cyclone 1 and cyclone 2. The first originated in latitude 39 $^\circ$ S on 02/05/2001 and the second, at latitude 27 $^\circ$ S on 04/05/2001. The first cyclone formed at a latitude away from the second. However, this generated a track wind along the coast who met the track formed by the second cyclone which probably potentiated the effect and intensity of the storm surge that hit the state of Santa Catarina. According to Innocentini, Oliveira e Cunha Prado (2003), the wave field intensivity was caused by the combined effect of these two tropical cyclones, since individually each cyclone and would not have the necessary fetch and duration to cause waves that intensity.

Because of the fact of the occurrence of two simultaneous extratropical cyclones this event was highlighted and its period of operation was simulated in waters near the coast using the SWAN model.

3.3.3 Model description

SWAN (Simulating Waves Nearshore) is a model of third generation wave to obtain realistic estimates of wave parameters in coastal areas, lakes and estuaries from wind data, bathymetry and currents (BOOIJ; RIS; HOLTHUIJSEN, 1999; RIS; HOLTHUIJSEN; BOOIJ, 1999). The model is based on equilibrium equation of wave action. This equation includes each term source: wind input, the nonlinear interactions, white-capping, friction in the background and induced break deep. In this study we used the 41.01 version of the SWAN model.

The grid used in the southern region is curvilinear and has 305 956 (892 $\times$ 343) cells with high resolution of approximately 0.5 km off the coast and low resolution of approximately 1.5 km

in deep water, rotated at 45 ° (Fig. 3.7). The area is approximately 286 000 km^2, covering the entire coastal area of Rio Grande do Sul and part of Uruguay and the state of Santa Catarina. The bathymetry for this grid is composed only of data of the General Bathymetric Chart of the Oceans (GEBCO) resolution of 30″ × 30″. The model was used in non stationary way, with a 5 minute time step and wind data input every 3 hours.

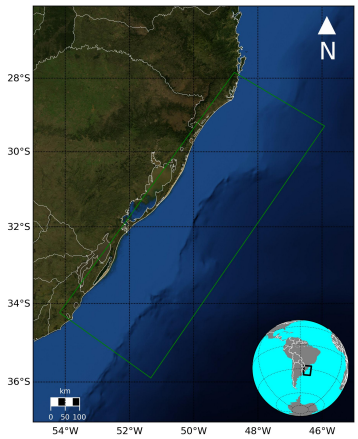

Figure 3.7: Study area showing the grid used for the simulation of the event 3.

Based on the elements described above, cyclone 1 belongs to the pattern III and Cyclone 2 to the pattern II. According Parise, Calliari e Krusche (2009), in the pattern II, a cyclone remains close to shore for longer, which causes a more localized impact. On the other hand, pattern III is responsible for a bigger rise in sea level (Machado et al. 2011). In the city of Rio Grande, wave heights varied between 0.7 and 2.28 m, in Tramandaí, between 0.53 and 2.13 m and in Garopaba, between 0.58 and 2.8 m (Fig. 3.11). We can observe that the increase is significant wave height occur from south to north along the southern coast of Brazil. In Rio Grande the largest wave heights occurred on 05.05.2001 at 07 h, in Tramandaí on 07.05.2001 at 13 h and Garopaba the peak was observed on 06.05.2001 at 07 h. The wind speed showed values between 3 and 12 m / s in Rio Grande, between 2.8 and 11 m / s in Tramandaí and between 0.6 and 15.3 m / s in Garopaba (Fig 3.12). Winds from S-SW were predominant in Rio Grande, Tramandaí and Garopaba (Fig. 3.13a, 3.13b and 3.13c). In the Rio Grande maximum wind speed occurred on 02.05.2001 at 13 h, in Tramandaí on 05.05.2001 at 01 h and in Garopaba, on 05.05.2001 at 19 h. The astronomical tide for the state of Rio Grande do Sul is classified as mixed semi-diurnal, with average amplitude of about 0.4 m (CALLIARI; TOZZI; KLEIN, 1998). Thus the events described may have been magnified and intensified because the meteorological tide in the region has high typical values.

To check the significant height and wind speed data obtained by the SWAN model, these form compared with satellite data obtained by altimetry. The comparison period corresponds to the days of operation of the two cyclones. These data were obtained through Globwave

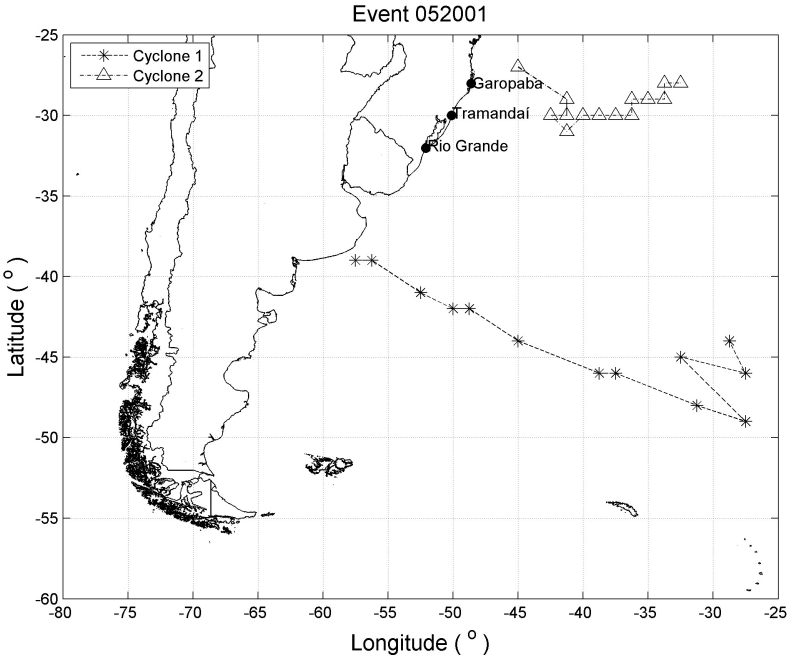

Figure 3.8: Simultaneous tracks of cyclones associated with the event 3. The spacing between consecutive asterisks and circles represents a period of three hours.

Figure 3.9: Impacts of storm surge and large waves that occurred in Florianopolis in May 2001. Source: DEDC-SC, 06/05/2001.

(http://globwave.ifremer.fr/), this project is an initiative of three years funded by the European Space Agency (ESA), to meet the needs of wave product users obtained by satellite around the world.

Table 3.4 and 3.5 show the significant height data and wind speed respectively, for three locations during the performance of the two cyclones with the time of the satellite measurements and the model.

Table 3.4: Significant height from satellite data and model during the period of operation of the two cyclones.

Local	Point	Satellite	Date	Time satellite	Time model	Hs satellite (m)	Hs model (m)
Garopaba (SC)	-43.91, -30.41	GEOSAT Follow-On	02/05/2001	18:24:57	18	1.64	2.0820
Tramandaí (RS)	-52, -33.15	TOPEX	02/05/2001	09:33:45	10	2.10	1.5370
Rio Grande (RS)	-52, -33.15	TOPEX	02/05/2001	09:33:45	10	2.10	1.5370
Garopaba (SC)	-48.03, -27.84	ERS-2	03/05/2001	02:00:05	2	1.169	0.7349
Tramandaí (RS)	-50.47, -30.88	GEOSAT Follow-On	03/05/2001	08:22:18	8	1.63	0.7721
Rio Grande (RS)	-50.21, -31.38	GEOSAT Follow-On	03/05/2001	08:22:18	8	1.95	1.2310
Garopaba (SC)	-44.32, -26.09	TOPEX	04/05/2001	08:22:00	8	2.20	2.2930
Tramandaí (RS)	-53.02, -33.63	GEOSAT Follow-On	04/05/2001	19:04:06	19	1.60	1.6840
Rio Grande (RS)	-53.02, -33.63	GEOSAT Follow-On	04/05/2001	19:04:06	19	1.60	1.6840
Garopaba (SC)	-50.26, -31.16	TOPEX	05/05/2001	08:45:22	9	2.60	2.7740
Tramandaí (RS)	-50.26, -31.16	TOPEX	05/05/2001	08:45:22	9	2.60	2.7740
Rio Grande (RS)	-53.27, -33.83	TOPEX	05/05/2001	18:41:20	19	2.20	1.7570
Garopaba (SC)	-49.11, -29.17	ERS-2	06/05/2001	02:05:26	2	5.94	3.2370
Tramandaí (RS)	-48.96, -29.74	ERS-2	06/05/2001	02:05:16	2	5.78	3.5560
Rio Grande (RS)	-48.5, -31.42	ERS-2	06/05/2001	02:04:48	2	5.86	3.9870
Garopaba (SC)	-48.4, -27.61	GEOSAT Follow-On	07/05/2001	19:09:16	19	3.64	3.1870
Tramandaí (RS)	-49.7, -30,18	GEOSAT Follow-On	07/05/2001	19:10:02	19	2.879	2.5370
Rio Grande (RS)	-51.09, -32.8	GEOSAT Follow-On	07/05/2001	19:10:49	19	2.439	2.3340

Table 3.5: Wind speed from satellite data and the model during the actuation of the two cyclones.

Local	Point	Satellite	Date	Time satellite	Time model	Wind satellite (m/s)	Wind model (m/s)
Garopaba (SC)	-43.91, -30.41	GEOSAT Follow-On	02/05/2001	18:24:57	18	8.14	8.0602
Tramandaí (RS)	-52, -33.15	TOPEX	02/05/2001	09:33:45	10	13.4	11.1504
Rio Grande (RS)	-52, -33.15	TOPEX	02/05/2001	09:33:45	10	13.4	11.1504
Garopaba (SC)	-48.03, -27.84	ERS-2	03/05/2001	02:00:05	2	7.759	7.0375
Tramandaí (RS)	-50.47, -30.88	GEOSAT Follow-On	03/05/2001	08:22:18	8	5.73	6.8497
Rio Grande (RS)	-50.21, -31.38	GEOSAT Follow-On	03/05/2001	08:22:18	8	7.009	7.9824
Garopaba (SC)	-44.32, -26.09	TOPEX	04/05/2001	08:22:00	8	9,90	11.0984
Tramandaí (RS)	-53.02, -33.63	GEOSAT Follow-On	04/05/2001	19:04:06	19	8.509	7.4254
Rio Grande (RS)	-53.02, -33.63	GEOSAT Follow-On	04/05/2001	19:04:06	19	8.509	7.4254
Garopaba (SC)	-50.26, -31.16	TOPEX	05/05/2001	08:45:22	9	11.1	8.54
Tramandaí (RS)	-50.26, -31.16	TOPEX	05/05/2001	08:45:22	9	11,1	8.54
Rio Grande (RS)	-53.27, -33.83	TOPEX	05/05/2001	18:41:20	19	8	7.9382
Garopaba (SC)	-49.11, -29.17	ERS-2	06/05/2001	02:05:26	2	15.32	12.4278
Tramandaí (RS)	-48.96, -29.74	ERS-2	06/05/2001	02:05:16	2	15.98	12.8040
Rio Grande (RS)	-48.5, -31.42	ERS-2	06/05/2001	02:04:48	2	16.78	13.7334
Garopaba (SC)	-48.4, -27.61	GEOSAT Follow-On	07/05/2001	19:09:16	19	6.169	7.7646
Tramandaí (RS)	-49.7, -30,18	GEOSAT Follow-On	07/05/2001	19:10:02	19	3.93	4.3403
Rio Grande (RS)	-51.09, -32.8	GEOSAT Follow-On	07/05/2001	19:10:49	19	5.339	4.8383

Figure 3.10: Impacts of storm surge and large waves that occurred in Itapoá in May 2001. Source: DEDC-SC, 06/05/2001.

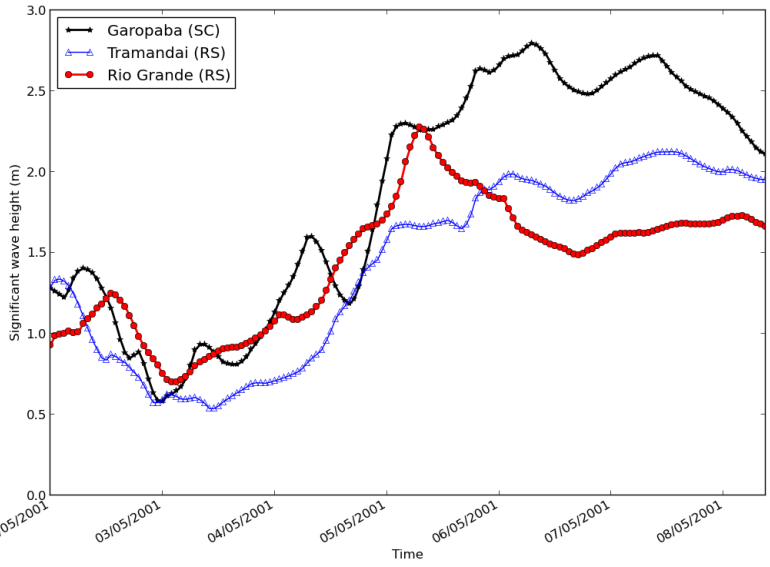

Figure 3.11: Significant wave height for the three locations during the event May 2001.

We observed that the most significant wave height and wind speed measurements from the satellite have values above the measurements from the model.

Because it is an extreme event caused by the actions of two tropical cyclones expected that the model measurements were closer to the satellite measurements which was not observed in this study. Instead there was an underestimation of model values relative to the satellite values for significant wave height data and the wind speed.

Using data from the Superintendence of Ports and Waterways (SPH), we obtained a maxi-

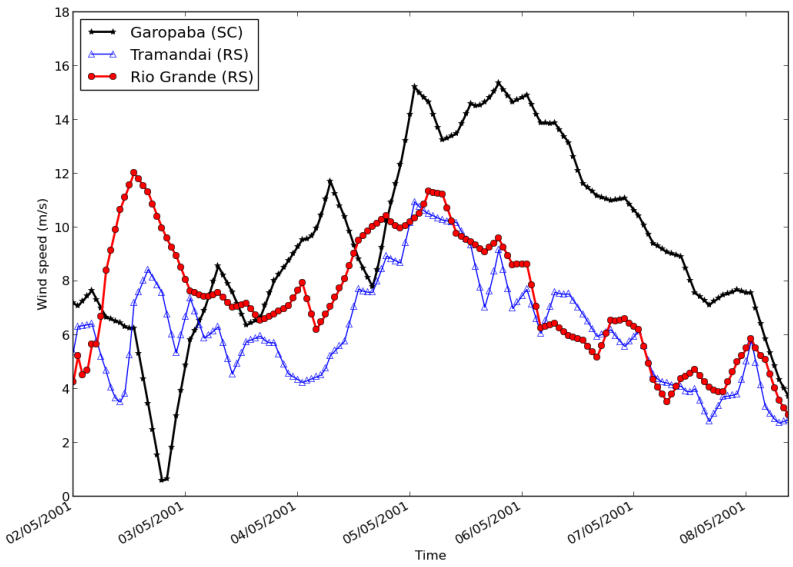

Figure 3.12: Wind speed for the three locations during the event of May 2001.

mum level rise from meteorological forcing (storm surge) of 0.64 m for the region Tramandaí on 05.05.2001 at 12:30 h, where the pressure in the center of the cyclone was 998.9 mbar. The value of storm surge for other locations was not calculated, since no data were available.

Synoptic features

The first cyclone originated on day 02 near latitude 40 ° S (Fig. 3.14a) shifting to southeast (Pattern III). On day 03, the winds intensified towards SW (Fig. 3.14b). This day was the lowest pressure recording in the center of the cyclone of 990 mbar and from day 04, the winds associated took the SE direction (Fig. 3.14c). Another low pressure center near latitude 27 ° S also observed which moves eastward (Pattern II). On day 05, trail wind near the coast (Fig. 3.14d) was formed and it was intensified in the days 06 and 07 (Fig. 3.14e and Fig. 3.14f), when the lowest pressure recorded in the center of the cyclone was 998 mbar, losing power in the next two days (Fig. 3.14g and Fig. 3.14h).

3.4 Conclusions

We have calculated the tracks of extatropical cyclones and classified them into 3 patterns. Pattern III is the most common (41.4%) with a higher incidence of events appearing in May. This agrees with the period of largest number of occurrences of coastal storms, as observed by Gan e Rao (1991). It was found that the prevailing winds of the patterns I, II and III were, respectively,

(a) Rio Grande

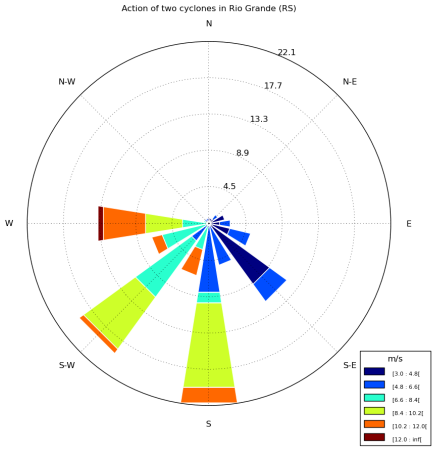

(b) Tramandaí

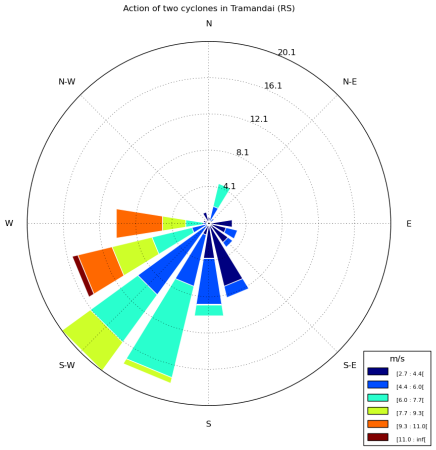

(c) Garopaba

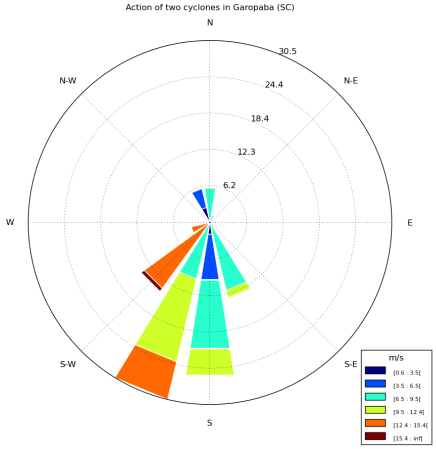

Figure 3.13: Wind direction and speed of the event of May 2001 in: a) Rio Grande, b) Tramandaí and c) Garopaba.

(a) (b) (c) (d)

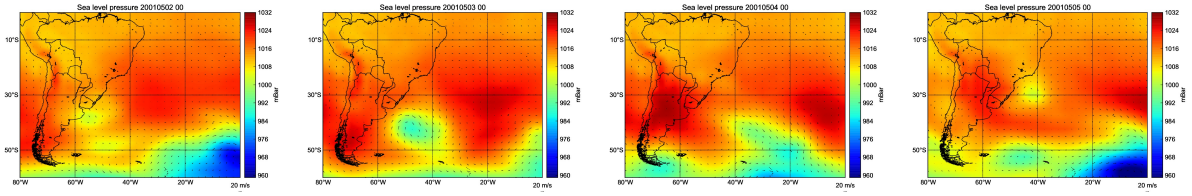

(e) (f) (g) (h)

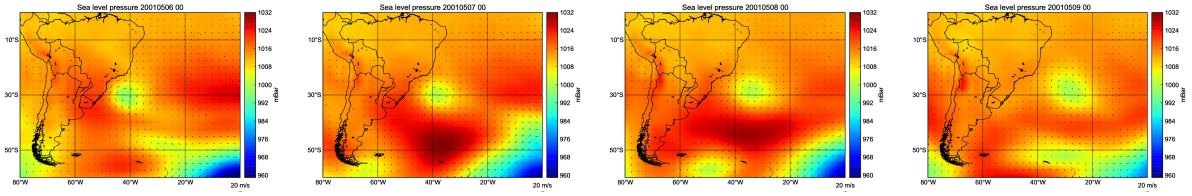

Figure 3.14: Synoptic situation of atmospheric pressure at sea level (mbar) and wind field (m/s) each hour for the event in May 2001.

NE, SW and SW in all three locations. The highest values of mean and maximum wave height are associated with patterns II and III, which are the most erosive and that generate the highest elevations in the sea level, respectively.

With the tracks calculated and classified into the three patterns, we determined the total number of events and analyzed the characteristics of significant wave heights and wind in the cities of Rio Grande, Tramandaí and Garopaba. We found that the largest values of wave heights are associated with patterns II and III (87.5%), especially the latter.

Considering the 28 events, we obtained a good overall correlation between data of significant wave height and wind speed. However, in some cases, associated with greatest significant wave heights, this correlation was not present. This may be related to the extension of the runway wind, as well as the duration of the wind, which varied significantly during the storm.

The event number 3, of May 2001 stood out from the others by presenting the simultaneous occurrence of two cyclones and by causing major damage to the coastlines in several cities. This event generated significantly higher values of maximum and average wave height. We have found that wave height and wind speed were significantly higher in the region of Garopaba, during the event. There was also evidence of a storm surge in the state of Santa Catarina. We found also that the event of May 2001 produced maximum significant wave height that overcame in roughly 10% all the other events (with exception to event 28) in all 11 years analyzed. These observations suggest the study of phenomena with similar characteristics of event 3 as a future topic investigation.

Acknowledgements

The first author acknowledges financial support by CAPES, Brazil, through the Project Edital Capes Ciências do Mar 09/2009. The second author has done part of the research on this article while a member of the EU Project FP7-295217, HPC-GA. His research was supported by the Basque Government through the BERC 2014-2017 program an by the Spanish Ministry of Economy and Competitiveness MINECO: BCAM Severo Uchoa excellence accreditation SEV-2013-0323.

References

BERNHARDT, J. E.; DEGAETANO, A. T. Meteorological factors affecting the speed of movement and related impacts of extratropical cyclones along the U.S. east coast. *Natural Hazards*, v. 61, n. 3, p. 1463–1472, jan 2012. ISSN 0921-030X. Disponível em: <http://link.springer.com/10.1007/s11069-011-0078-0>.

BITENCOURT, D. P. et al. Relating winds along the Southern Brazilian coast to extratropical cyclones. *Meteorological Applications*, v. 18, n. 2, p. 223–229, jun 2011. ISSN 13504827. Disponível em: <http://doi.wiley.com/10.1002/met.232>.

BOOIJ, N.; RIS, R. C.; HOLTHUIJSEN, L. H. A third-generation wave model for coastal regions: 1. Model description and validation. *Journal of Geophysical Research*, v. 104, n. C4, p. 7649, 1999. ISSN 0148-0227. Disponível em: <http://doi.wiley.com/10.1029/98JC02622>.

CALLIARI, L. J.; TOZZI, H. A. M.; KLEIN, A. H. F. Beach Morphology and Coastline Erosion Associated with Storm Surges in Southern Brazil-Rio Grande to Chuí, RS. *Anais da Academia Brasileira de Ciências*, v. 70, n. 2, p. 231–247, 1998.

CATTO, J. L.; SHAFFREY, L. C.; HODGES, K. I. Northern Hemisphere Extratropical Cyclones in a Warming Climate in the HiGEM High-Resolution Climate Model. *Journal of Climate*, v. 24, n. 20, p. 5336–5352, oct 2011. ISSN 0894-8755. Disponível em: <http://journals.ametsoc.org/doi/abs/10.1175/2011JCLI4181.1>.

CHAMPION, A. J. et al. Impact of increasing resolution and a warmer climate on extreme weather from Northern Hemisphere extratropical cyclones. *Tellus A*, v. 63, n. 5, p. 893–906, oct 2011. ISSN 02806495. Disponível em: <http://tellusa.net/index.php/tellusa/article/view/15876>.

DRAGANI, W. et al. Are wind wave heights increasing in south-eastern south American continental shelf between 32° S and 40° S? *Continental Shelf Research*, Elsevier, v. 30, n. 5, p. 481–490, mar 2010. ISSN 02784343. Disponível em: <http://linkinghub.elsevier.com/retrieve/pii/S0278434310000117>.

DRAGANI, W. C. et al. Synoptic patterns associated with the highest wind-waves at the mouth of the Río de la Plata estuary. *Dynamics of Atmospheres and Oceans*, Elsevier B.V., v. 61-62, p. 1–13, jun 2013. ISSN 03770265. Disponível em: <http://dx.doi.org/10.1016/j.dynatmoce.2013.02.001 http://linkinghub.elsevier.com/retrieve/pii/S0377026513000213>.

GAN, M. A.; RAO, V. B. Surface Cyclogenesis over South America. *Monthly Weather Review*, v. 119, n. 5, p. 1293–1302, 1991.

HADLOCK, R.; KREITZBERG, C. W. The Experiment on Rapidly Intensifying cyclones over the Atlantic (ERICA) Field Study: Objectives and Plans. *Bulletin of the American Meteorological Society*, v. 69, n. 11, p. 1309–1320, nov 1988. ISSN 0003-0007. Disponível em: <http://journals.ametsoc.org/doi/abs/10.1175/1520-0477(1988)069<1309:TEORIC>2.0.CO;2 http://journals.ametsoc.org/doi/abs/10.1175/1520-0477%281988%29069%3C1309%3ATEORIC%3E2.0.CO%3B2>.

INNOCENTINI, V.; OLIVEIRA, F. A.; Cunha Prado, S. C. S. Modelo de ondas aplicado ao caso 5-8 de maio de 2001. *Revista Brasileira de Meteorologia*, v. 18, n. 1, p. 97–104, 2003.

KALNAY, E. et al. The NCEP/NCAR 40-Year Reanalysis Project. *Bulletin of the American Meteorological Society*, v. 77, n. 3, p. 437–471, mar 1996. ISSN 0003-0007. Disponível em: <http://journals.ametsoc.org/doi/abs/10.1175/1520-0477(1996)077<0437:TNYRP>2.0.CO;2>.

MACHADO, A. A. et al. Historical assessment of extreme coastal sea state conditions in southern Brazil and their relation to erosion episodes. *Pan-American Journal of Aquatic Sciences*, v. 5, p. 105–114, 2010.

PARISE, C. K.; CALLIARI, L. J.; KRUSCHE, N. Extreme storm surges in the south of brazil: atmospheric conditions and shore erosion. *Brazilian Journal of Oceanography*, v. 57, n. 3, p. 175–188, 2009.

RIS, R. C.; HOLTHUIJSEN, L. H.; BOOIJ, N. A third-generation wave model for coastal regions: 2. Verification. *Journal of Geophysical Research*, v. 104, n. C4, p. 7667, 1999. ISSN 0148-0227. Disponível em: <http://doi.wiley.com/10.1029/1998JC900123>.

ROCHA, R. P.; SUGAHARA, S.; SILVEIRA, R. B. da. Sea Waves Generated by Extratropical Cyclones in the South Atlantic Ocean: Hindcast and Validation against Altimeter Data. *Weather and Forecasting*, v. 19, n. 2, p. 398–410, apr 2004. ISSN 0882-8156. Disponível em: <http://journals.ametsoc.org/doi/abs/10.1175/1520-0434(2004)019<0398:SWGBEC>2.0.CO;2>.

SELUCHI, M. E. Diagnóstico y prognóstico de situaciones sinópticas conducentes a desarrollos ciclónicos sobre el este de Sudamérica. *Geofísica Internacional*, v. 34, p. 171–186, 1995.

SINCLAIR, M. R. An Objective Cyclone Climatology for the Southern Hemisphere. *Monthly Weather Review*, v. 122, n. 10, p. 2239–2256, 1994.

SINCLAIR, M. R. A Climatology of Cyclogenesis for the Southern Hemisphere. *Monthly Weather Review*, v. 123, n. 6, p. 1601–1619, 1995.

TOLMAN, H. L. *User manual and system documentation of WAVEWATCH-III version 1.18*. Washington, DC, 1999. 110 p.

TOZZI, H. A. M.; CALLIARI, L. J. Trajetórias e distribuição das tempestades extratropicais e o impacto na costa do Rio Grande do Sul. In: *VII Congresso da Associação Brasileira de Estudos do Quaternário*. Porto Seguro - BA: [s.n.], 1999. p. 1–3.

4 Uniform spatial representation of global ocean wave fields obtained from Satellite and comparison with model data

Representação espacial uniforme de campos globais de onda oceânica obtidos a partir de dados de satélite e comparação com dados de modelo

Heitor Perotto[1], Leandro Farina[2,3] and Nelson Violante-Carvalho[4]

[1] *Instituto de Geociências, Universidade Federal do Rio Grande do Sul, Porto Alegre, Brazil*,

[2] *Instituto de Matemática e Estatística and Centro de Estudos de Geologia Costeira e Oceânica, CECO Universidade Federal do Rio Grande do Sul, Porto Alegre, Brazil*,

[3] *Basque Center for Applied Mathematics (BCAM), Bilbao, Basque Country, Spain*

[4] *Programa de Engenharia Naval e Oceânica, PEnO, Rio de Janeiro, Brazil*
Universidade Federal do Rio de Janeiro.

Abstract

An algorithm for representing irregular satellite data obtained from ASAR uniformly in space is introduced and comparison with WAVEWATCH III model data is carried out. Swell global data for 2007 are analysed using statistical parameters such as bias and scattering index. Satellite data showed a great spatial uniformity compared with model data. Underestimation of swell height by the model in the tropics and at specific regions high latitudes are found.

Keywords: swell, surface water waves, irregular data, satellite sensing, algorithms, mathematical models.

Resumo

Um algoritmo para a representação de dados de satélite irregulares obtidos a partir do sensor ASAR dispostos uniformemente no espaço é introduzido e uma comparação com dados do modelo WAVEWATCH III é realizada. Os dados globais de altura de swell para 2007 são analisados usando parâmetros estatísticos, como viés e índice de espalhamento. Os dados de satélite mostraram uma grande uniformidade espacial em comparação com os dados do modelo. Subestimação da altura de swell pelo modelo nos trópicos e em regiões específicas de altas latitudes são encontradas.

Palavras-chave: swell, ondas superficiais, dados irregulares, detecção de satélites, algoritmos, modelos matemáticos.

4.1 Introduction

A Synthetic Aperture Radar (SAR) inboard satellites can be used to measure directional wave spectrum. In its so called wave mode, small areas of around 5 by 5 km are imaged along the satellite ground track, yielding thousands of wave spectra per orbit with global coverage. Our knowledge about wave climate and wave propagation has increased substantially since the launch of ERS-1 in the early 1990s (see a thoroughly discussion about the SAR wave mode in Hasselmann et al. (2013)).

Investigations about wave climate have increased and satellite data have been increasingly employed. Satellite observations have a global coverage and also provide information with a high level of accuracy. Along with satellite data, numerical modelling can be used as a tool for providing numerical predictions. Despite the irregular spatial and temporal coverage of satellite wave data, these records are supposedly the closest measurements to the true sea state. The results of a model for forecasting or hindcasting wave fields provide a regular, homogeneous field in time and space. However, they are subject to many uncertainties, such as the quality of wind input and the model physics and configuration. Thus, a comparison of data obtained by satellite with the model data model becomes very useful to determine the real sea state.

Young (1999) examined a data set covering a 10-year period acquired from a combination of satellite data and model predictions obtained in order to establish wind and wave global climates. The results were presented in terms of average monthly statistics for significant wave height, peak and average wave period, wave direction and wind speed and direction. The results clearly showed zonal variation for the wind speed and wave height, to extreme conditions that occur at high latitudes. It was observed that the swell generated from storms in the Southern Ocean penetrates across the Indian Ocean, South Pacific and South Atlantic. During the southern hemisphere winter, the swell still enters the North Pacific. It was also found that the western side of most continents have noticeably more intense wave climates than the east side; this is a result

of the generation of longer fetches that exist on the West Coast and the direction of propagation of prevailing winds.

Reguero et al. (2012) used a global set of wave data from 1948 to 2008. Employing a calibration method, the data set have been fixed based on altimeter data from 1992 to 2008. The quality of the corrected results were compared with measurements from buoy and satellite altimeter. The diagnostic statistics showed an agreement both with scatter data as the statistical distribution of wave heights, indicating that the reanalysis adequately reflects the characteristics of the waves from satellite data between 1992 and 2008.

A feasibility study to use wind speed and significant wave height measurements of simultaneous sources of scatterometer and altimeter satellite to observe the pattern of spatial and seasonal distribution of the dominant areas of swell and wind in all oceans has been proposed by Chen et al. (2002). Two normalised indices related to energy were presented. Based on these, global probability and intensity statistics for swell and wind were obtained. Regions with intense wave growth were observed in the Pacific, Northwest Atlantic, Southern Ocean and the Mediterranean Sea. The observed seasonality is somewhat different between the climates of swell and wind.

An analysis using a set of satellite altimeter data was carried out by Izaguirre et al. (2011), which provided a global comprehensive level for the year of 1992. An analysis of non-stationary extreme values, modelling the seasonal and inter annual variations was employed to characterise extreme significant wave height.

Ren et al. (2011) compared six years of ENVISAT satellite ASAR spectrum data with one-dimensional wave spectra obtained from 44 buoys in the Northern Pacific. They found that the ASAR wave spectra tend to significantly underestimate the significant wave heights at high wind speeds and overestimate them at low wind speeds.

ENVISAT level 2 (ASA _WVW_2P) wave spectra data were compared with other altimeter and buoys measurements, located in the Gulf of Mexico and in the Pacific Ocean, and with wave models by Li e Saulter (2012). This indirect comparison was made for 14 months, from November 2007 to December 2008. The ASAR swell data proved to be consistent with the model and buoy data.

Stopa et al. (2016) used synthetic aperture radar data to identify swell sources and trajectories, allowing a statistically significant estimation of swell dissipation. They employed the whole ENVISAT mission (2003 - 2012) to find suitable storms with swells (with periods T such that $13 < T < 18$ s) that were observed several times along their propagation. The analysis reveals that swell dissipation weakly correlates with the wave steepness, wind speed, orbital wave velocity, and the relative direction of wind and waves. Although several negative dissipation rates

are found, there are uncertainties in the SAR-derived swell heights and dissipation rates. An acceptable range of the swell-dissipation rate is -0.1 to 6×10^{-7} m^{-1} with a median of 1×10^{-7} m^{-1}.

One of the shortcomings of data obtained by satellite is the irregular spatial distribution inherent to these. In this work, we present an algorithm that reallocate the wave data in a uniform grid without the use of averages. Thus, only actual, ponctual measured values are plotted and analysed.

In this work we used global data for the whole year of 2007. The data used was the directional wave spectra (ASA _WVW_2P) obtained by the ENVISAT satellite of the European Space Agency (ESA) through the ASAR sensor. These data were compared with WAVEWATCH III (WW3) model data, developed for the same period. The ocean variable analysed is swell for a global grid.

In the next section we describe the data set used. In section 4.3, we present give details of the algorithm for the uniform data representation while the overall results on the wave fields are presented and discussed in section 4.4. The conclusion remarks of the article are given in section 4.5.

4.2 Satellite and model wave data

In this section we describe the data we have worked with.

4.2.1 Satellite data

ENVISAT was launched in March 2002 by the European Space Agency to follow on its predecessors ERS-1 & 2. Its main objective was to provide atmosphere, ocean, land and ice data at monitoring global warming, the degree of air pollution and natural disaster risks. ENVISAT carried ten instruments on board, with optical sensors and active sensors, and among them its main asset, the Advanced Synthetic Aperture Radar (ASAR) sensor. The ENVISAT mission ended on 8 April 2012, following the unexpected loss of contact with the satellite.

The ASAR sensor is an enhanced version of the SAR instrument that was already in operation on board satellites ERS-1 and ERS-2. This has a 10 m long antenna, and operates in five different modes: image mode, mode alternating polarisation wide band mode, monitor mode, and global wave mode. The sensor in wave mode produces small 5 km $\times$ 5-10 km images, called *imagettes*, of the sea surface. These images are processed to derive the wave spectrum of the sea surface and hence the wavelength, period, height and direction of the waves. The processing

of Level 2 data uses an algorithm developed and implemented by IFREMER/CERSAT ((JOHNSEN et al., 2006)).

4.2.2 The wave model

The WW3 wave model (TOLMAN, 1999) developed by NOAA / NCEP solves the spectral action energy conservation equation. The physical model includes wave growth, dissipation due to wave breaking in the background, refraction, advection and nonlinear interactions.

In our implementation, the WW3 model is used with spatial resolution of $0.6^\circ \times 0.6^\circ$ for latitude and longitude respectively and temporal resolution of 3 hours. The simulations are performed in a global domain 70° S to 70° N and 0 to 360° E. As input the surface wind components (U and V) predictions and ice cover calculated by the NCEP Climate Forecast System Reanalysis (CFSR) are used.

We used data from the spectral partitions provided by the model. The WW3 model has both point and field output options available to provide quantitative descriptions of these individual spectral partitions. The analysis of the wave system described in (HANSON; PHILLIPS, 2001) is applied.

The spectral partitioning method subdivides the directional spectrum into a number of overlapping wave components (partitions), each of which can be characterised by average parameters such as significant height, mean frequency, direction of propagation, and directional scattering.

Regardless of the method used, all the partitioning schemes follow the following logic: isolation of the peaks of energy, identification and combination of peaks of energy, removal of partitions with low energy and statistics of the main parameters of waves.

4.3 Uniform spatial representation

The allocation of the satellite data, which is irregular in space, into a regular mesh is carried out by an algorithm with two procedures. The first rearrange the satellite data onto the model regular grid, placing the satellite data closest to its original irregular coordinates. When two satellite measurements are found, within the specified period of time (taken here as one month), in the same cell of the model mesh, the largest measured value is selected. Let $V_{sat-orig}(\mathbf{x}, t)$ denote the variable V measured by the satellite at a point $(\mathbf{x}, t) = (x, y, t)$ on latitude x, longitude y and time t. Let also $lat(i), lon(j)$ be the latitudes and longitudes of the model's horizontal physical mesh of size $N \times M$. This algorithm generates a regular submesh of size $N_b \times M_b$,

which can coincide with the model original mesh, particularly when the amount of satellite data over one month is sufficiently large and homogeneously distributed.

Procedure 1 is described below.

Data: Satellite data over a month and model mesh

Result: Satellite data $V_{sat-reg}$ arranged on regular submesh

for $(\mathbf{x}, t) \in$ *Sat. global domain* $\times$ *one month* **do**

  $count(i, j) = false$;

  for $i = 1, ... N - 1, j = 1, ..., M - 1$ **do**

    if $x > lat(i)$ *and* $x \leq lat(i + 1)$ **and** $y > lon(j)$ *and* $y \leq lon(j + 1)$ **then**

      if $count(i, j) = true$ **then**

        if $V_{sat-reg}(i, j, date(i, j)) < V_{sat-orig}(\mathbf{x}, t)$ **then**

          $date(i, j) = t$;

          $V_{sat-reg}(i, j, date(i, j)) = V_{sat-orig}(\mathbf{x}, t)$

        else

          increment $i; j$

        end

      else

        $date(i, j) = t$;

        $V_{sat-reg}(i, j, date(i, j)) = V_{sat-orig}(\mathbf{x}, t)$;

        $count(i, j) = true$

      end

    end

  end

end

Procedure 1: Reallocate satellite data in regular mesh.

The second procedure compares the dates of the satellite measurements with model dates. This selects only the model dates that have a corresponding date with the satellite. Let $k = 1, ..., T$ be the dates computed by the model during the month under study. Algorithm 2 is described as follows.

Data: Dates where satellite data exists, spatial submesh and model temporal mesh

Result: Model data $V_{mod-reg}$ on the submesh and on selected dates

for $k = 1, \ldots, T$ **do**

  for $i = 1, \ldots N_b - 1, j = 1, \ldots, M_b - 1$ **do**

    if $date(i,j) > k$ *and* $date(i,j) \leq k+1$ **then**

      $V_{mod-reg}(i,j,date(i,j)) = V_{mod-orig}(i,j,k)$

    end

  end

end

Procedure 2: Selects the valid dates on the model data.

As a result of the algorithm, the variables $V_{mod-reg}$ and $V_{sat-reg}$ can then be compared on the same spatio-temporal framework. In our comparison, we have computed swell height.

4.4 Swell Height

To analyse the data obtained from ENVISAT, through the ASAR sensor, we carried out a comparison with data obtained by the WW3 model. The swell height was obtained and simulated for the whole year of 2007. For the graphical presentation of results, we selected a single month for each of the four seasons.

Besides the values of swell heights, we also computed the bias Eq.(4.1) and the scattering index Eq.(4.2) from our dataset. Specifically, we have used:

$$V = M - S, \tag{4.1}$$

$$SI = \frac{\sqrt{\frac{1}{n}\sum_{i=1}^{n}(M_i - S_i)^2}}{\bar{S}} \tag{4.2}$$

where V is the bias, SI is the scatter index and n is the number of observations. M stands for model and S for satellite satellite measurements. The bar over S represents spatial average.

Each value of the swell height, as well as the bias and the scatter index is represented by a pixel, with its corresponding latitude and longitude, in the maps of all figures below.

The satellite wavelength measurements range is 100-400 m, which is equivalent to periods of 8-16 s. Thus we selected a corresponding data by the model which originally computes a wider range of periods, greater than 16 s and less than 8 s.

It is observed from the satellite and model data in figures 4.1 and 4.2 that the largest values of swell height are located near latitude 60 $^\circ$ for both the Southern Hemisphere (SH) and the Northern Hemisphere (NH), corroborating with previous findings on ocean wave climate (YOUNG, 1999; IZAGUIRRE et al., 2011). In the months corresponding to winter and fall,

in the respective hemispheres, these values intensify. Analysing both dataset we notice that the

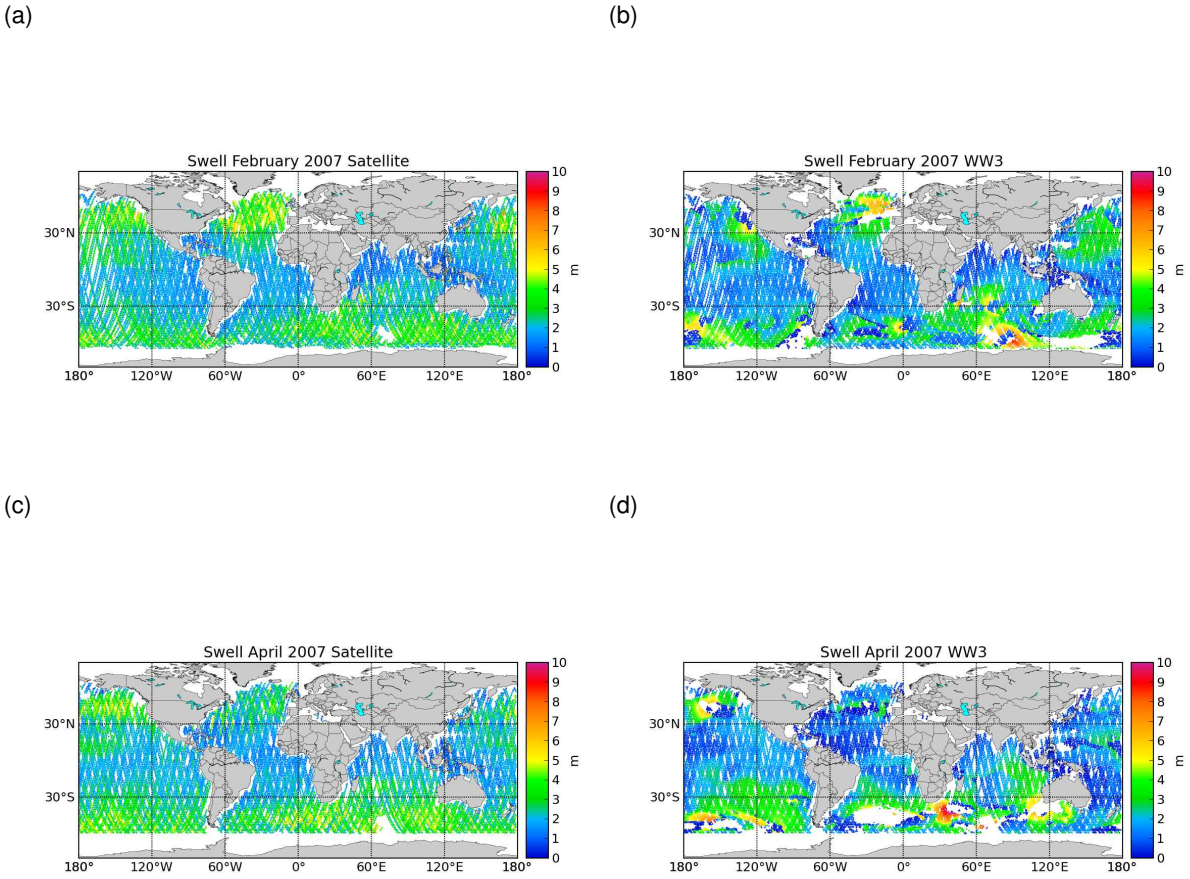

Figure 4.1: Global distributions of swell height in meters by the satellite and model for the months of February and April, 2007.

SH show a significant rougher sea state than the NH. In particular, stronger swell fields are observed in the South Pacific, Southern Africa and Southern and Eastern Australia in the autumn and winter of the SH. Important high swell also occur in the Southwestern Atlantic and is seen from the model data of April (figure 4.1) and in the model and satellite data of July (figure 4.2). These fields are associated with the frequent occurrence of extra-tropical cyclones in the South America, in the fall of the SH. In the NH, the highest waves are found in the North Pacific and North Atlantic during the winter, as shown in figure 4.1.

Satellite measurements show very clearly high swell heights in the Northwestern Indian Ocean in the North Hemisphere late spring (June) and summer (figure 4.2). This can be explained by strong southwest winds that develops near the coast of Africa and is associated with the Asian summer monsoon Asian (YOUNG, 1999). The negative bias of July in this region, shown in figure 4.3, indicates the model did not accurately pick up this phenomenon. The largest bias in the comparison satellite-model, presented in figure 4.3, were observed at high latitudes, spe-

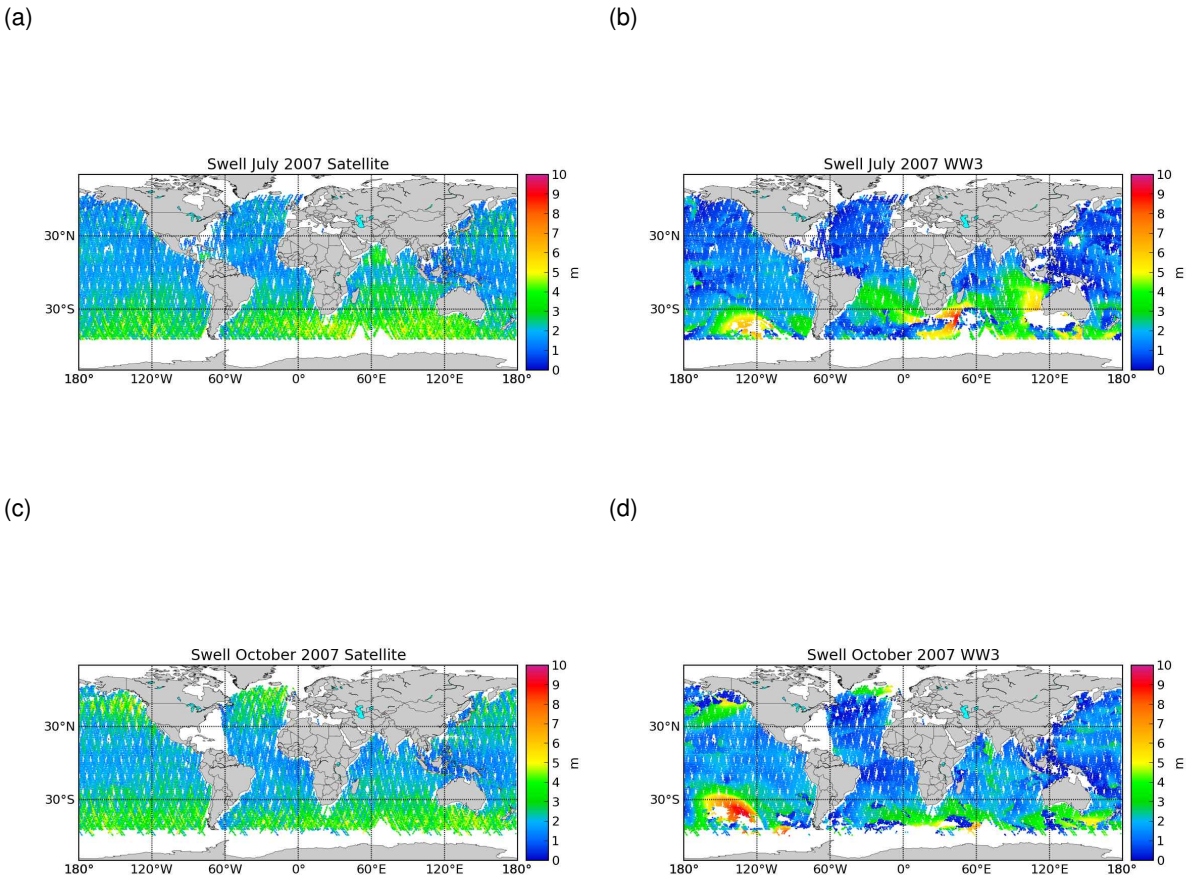

Figure 4.2: Global distributions of swell height in meters by the satellite and model for the months of July and October, 2007.

cially in the SH. In figure 4.4, we see that the scatter index is below 0.5, almost everywhere. In some regions, these values were close to 1. Higher values (greater than 1) were observed in the North Atlantic, South Pacific and Northern Australia.

The bias we found presents complex characteristics for the year analysed. We could infer that from the months of between February and April, the highest values of bias, meaning overestimation by the model, are predominantly positive with a remarkable exception in regions of the Atlantic in latitude range 40-45 $^\circ$ S and also in 40-45 $^\circ$ N, including the North Pacific. In the months of July and October, the same extra-tropical range show underestimation by the model in the Atlantic, and South Indian Ocean. In the tropics, our results show less intense but more extensive areas with negative bias, and thus model underestimation of swell heights apparently contradicting previous findings of systematic overestimation of wave heights by numerical wave models (RASCLE et al., 2008). This may be related to the fact that in the algorithm used in this work, when more than one satellite measurement is found in the same cell of the model mesh for the same period of time, taken here as one month, the highest value is selected and a new

value computed by the model is also picked up within the shortest time tolerance. Thus, this procedure is done without compromising the nearness in time for each two values compared.

(a)

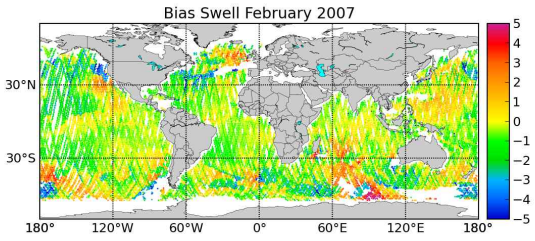

(b)

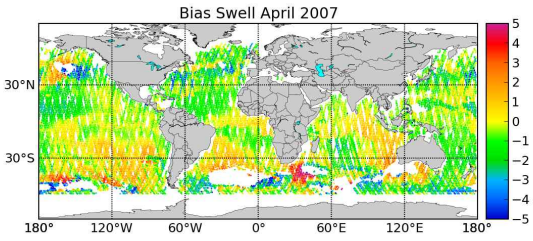

(c)

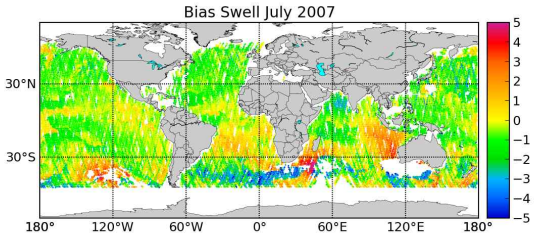

(d)

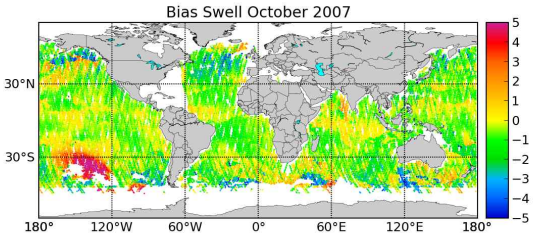

Figure 4.3: Global bias for all four seasons of 2007.

(a)

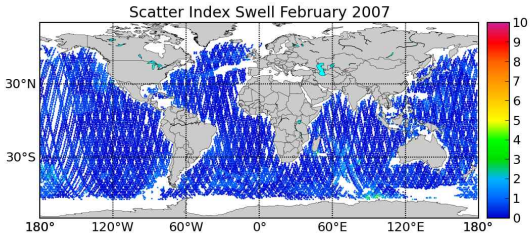

(b)

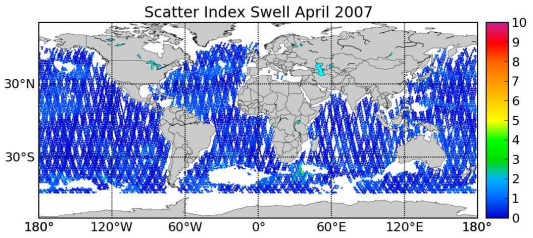

(c)

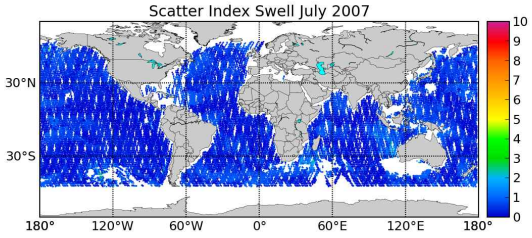

(d)

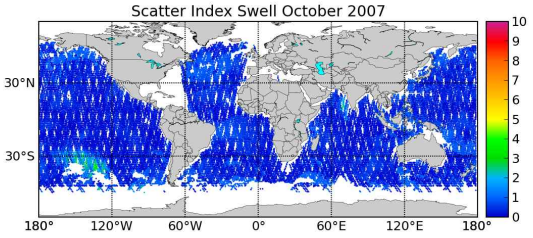

Figure 4.4: Global scattering index for all four seasons of 2007.

4.5 Conclusions

In this work an algorithm for representing irregular satellite wave data in a uniform mesh has been introduced. This procedure also allows the comparison between satellite and model data in the same point in space and time.

ENVISAT swell heights, obtained through the ASAR sensor have been compared with the swell computed by the WaveWatchIII. As an propositional work, a short-scale simulation of the wave model were performed for the entire year of 2007 and results for a month of each season have been analysed through bias and scatter index.

Known features of the global wave climate have been corroborated as well as specific findings for the year studied. In special, higher latitude regions where the model underestimate the measured swell heights have been identified. Further, it has been noticed that in the tropics, less intense but more extensive areas also present negative bias, and thus model underestimation of swell heights. These findings should provide additional insights for the ocean wave modelling community and indication of future model improvements and calibration.

The features of the uniform satellite representation introduced here must be further investigated and extended to other physical variables such as wave period and direction and a similar study as the one presented here should be carried out using a more comprehensive dataset, incorporating several years.

Acknowledgements

The first author acknowledges financial support by CAPES, Brazil, through the Project Edital Capes Ciências do Mar 09/2009. The second author has done part of the research on this article while a member of the EU Project FP7-295217, HPC-GA. His research was supported by the Basque Government through the BERC 2014-2017 program an by the Spanish Ministry of Economy and Competitiveness MINECO: BCAM Severo Uchoa excellence accreditation SEV-2013-0323.

References

CHEN, G. et al. A Global View of Swell and Wind Sea Climate in the Ocean by Satellite Altimeter and Scatterometer. *Journal of Atmospheric and Oceanic Technology*, v. 19, n. 11, p. 1849–1859, nov. 2002.

HANSON, J. L.; PHILLIPS, O. M. Automated Analysis of Ocean Surface Directional Wave Spectra. *Journal of Atmospheric and Oceanic Technology*, v. 18, n. 2, p. 277–293, feb 2001. ISSN 0739-0572. Disponível em: <http://journals.ametsoc.org/doi/pdf/10.1175/1520-0426(2001)018%3C0277:AAOOSD%3E2.0.CO%3B2>.

HASSELMANN, K. F. et al. *The ERS SAR wave mode: A breakthrough in global ocean wave observations*. Noordwijk: ESA Communications, 2013. 167–197 p. (ESA Special Publication, v. 1326).

IZAGUIRRE, C. et al. Global extreme wave height variability based on satellite data. *Geophysical Research Letters*, v. 38, n. 10, p. L10607, maio 2011.

JOHNSEN, H. et al. Envisat asar wave mode products - quality assessment and algorithm upgrade. In: ESA (Ed.). *SEASAR 2006, Advances in SAR Oceanography from ENVISAT and ERS missions*. Frascati, Italy: [s.n.], 2006.

LI, J.-G.; SAULTER, A. Assessment of the updated Envisat ASAR ocean surface wave spectra with buoy and altimeter data. *Remote Sensing of Environment*, Elsevier B.V., v. 126, p. 72–83, nov. 2012.

RASCLE, N. et al. A global wave parameter database for geophysical applications. Part 1: Wave-current-turbulence interaction parameters for the open ocean based on traditional parameterizations. *Ocean Modelling*, v. 25, n. 3-4, p. 154–171, jan 2008. ISSN 14635003. Disponível em: <http://linkinghub.elsevier.com/retrieve/pii/S1463500308001017>.

REGUERO, B. et al. A Global Ocean Wave (GOW) calibrated reanalysis from 1948 onwards. *Coastal Engineering*, Elsevier B.V., v. 65, p. 38–55, jul. 2012.

REN, Q. et al. Comparison and analysis of Envisat ASAR ocean wave spectra with buoy data in the northern Pacific Ocean. *Chinese Journal of Oceanology and Limnology*, v. 29, n. 1, p. 10–17, jan. 2011.

STOPA, J. E. et al. Swell dissipation from 10 years of Envisat ASAR in wave mode. *Geophysical Research Letters*, p. n/a–n/a, mar 2016. ISSN 00948276. Disponível em: <http://doi.wiley.com/10.1002/2015GL067566>.

TOLMAN, H. L. *User manual and system documentation of WAVEWATCH-III version 1.18*. Washington, DC, 1999. 110 p.

YOUNG, I. Seasonal variability of the global ocean wind and wave climate. *International Journal of Climatology*, v. 19, n. 9, p. 931–950, jul. 1999.

5 Sensibility of a model of regional waves the boundary conditions provided by global model and satellite

Sensibilidade de um modelo de onda regional na costa do Brasil usando condições de fronteira fornecidas por um modelo global e por satélite

Heitor Perotto[1] and Leandro Farina[2,3]

[1] *Instituto de Geociências, Universidade Federal do Rio Grande do Sul, Porto Alegre, Brazil*,

[2] *Instituto de Matemática e Estatística e Centro de Estudos de Geologia Costeira e Oceânica, CECO Universidade Federal do Rio Grande do Sul, Porto Alegre, Brazil*,

[3] *Basque Center for Applied Mathematics (BCAM), Bilbao, Basque Country, Spain*

Abstract

In order to check and compare the wave parameters of behaviour near coastal regions, a study is conducted based on six events, three located in the southern and another three in the northeastern Brazil between 2002 and 2009, prioritising events where the swell is dominant. For a more realistic comparison, these events were selected based on the range in which ENVISAT measured the wavelength. Model data from WAVEWATCH III (WW3) and satellite data were used as boundary conditions for the SWAN model. The two simulations are compared in time and space and at specific points located in shallow and deep water, for each event. It is observed that there is an excellent correlation shown by the Pearson correlation coefficient between the two simulations studied in both regions, particularly in the temporal and spatial analysis. In shallow and deep waters greater correlation is observed in the south. The results show that there is a great coherence between the two simulations with Pearson coefficient values above 0.8. It is

also found that the peak period for the simulation with WW3 data is underestimated in relation to the simulation with satellite data on all events.

Keywords: swell, ENVISAT, SWAN.

Resumo

Para verificar e comparar o comportamento dos parâmetros de ondas próximo a regiões costeiras, um estudo é conduzido com base em seis eventos, três localizados no sul e outros três no Nordeste do Brasil entre 2002 e 2009, priorizando eventos em que o swell é dominante. Para uma comparação mais realista, esses eventos foram selecionados com base no intervalo em que o ENVISAT mediu o comprimento de onda. Dados do modelo WAVEWATCH III (WW3) e dados de satélite foram usados como condições de contorno para o modelo SWAN. As duas simulações são comparadas no tempo e no espaço e em pontos específicos localizados em águas rasas e profundas, para cada evento. Observa-se que existe uma excelente correlação evidenciada pelo coeficiente de correlação de Pearson entre as duas simulações nas duas regiões estudadas, principalmente na análise espacial e temporal. Em águas rasas e profundas uma maior correlação é observada na região sul. Os resultados mostram que há uma grande coerência entre as duas simulações com valores de coeficiente de Pearson acima de 0,8. Verificou-se também que o período de pico para a simulação com dados da WW3 é subestimado em relação à simulação com dados de satélite em todos os eventos.

Palavras-chave: swell, ENVISAT, SWAN.

5.1 Introduction

The wave climate knowledge has become increasingly relevant given its impact on a wide range of activities such as shipping, fishing activity, leisure, coastal and offshore industry and coastal management. For this purpose the use of predictive models as well as satellite data have increased, as these are methods with low operating costs compared to field measurements. Thus, a comparison of data obtained by satellite with the model data used as a model input parameter serves as conditions to ascertain the accuracy of these measurements.

Comparisons between satellite data and mathematical models are common; for instance recent studies focused on the Australian region (GREENSLADE, 2001), Pacific Ocean (REN et al., 2011) and on the global domains (LI; HOLT, 2009; LI; SAULTER, 2012). In the South Atlantic, much fewer studies were carried out.

Rocha, Sugahara e Silveira (2004) analysed six extra-tropical cyclones formed in the Southwes-

tern Atlantic between April and September 1999. Using past events data from a third-generation wave model, they found values of wave heights up to 5 m during some events near the Brazilian coast. The comparison with the satellite altimetry data showed a systematic underestimation of 0.5 m in the significant wave height, relative to the model.

Poças et al. (2010) conducted a comparison of the directional wave spectra derived from radar images of the ENVISAT satellite with data from the wave model WAVEWATCH III (TOLMAN, 1999) and two buoys off the coast of Santa Catarina and Rio Grande do Sul, in southern Brazil. There was a substantial correlation between the significant wave height data measured in situ by buoys, WAVEWATCH III output and those obtained by digital processing of SAR images. However, the peak period values showed some disparity between the measurements from buoys and satellite and also between the data model and satellite. Thus, the bias and mean square error are greater.

Using the wave model SWAN, Guimarães, Farina e Toldo Jr. (2014), simulated extreme events generated by extratropical cyclones in the South Atlantic in the period 2000-2010 to check the impact on the coast of Rio Grande do Sul, Brazil. They compared the model with buoy data and statistical results showed that all three analysed wave parameters; significant wave height, peak period and direction peak had a good match with the reality in most of the cases studied, with correlation coefficients between 0.79 and 0.85. Six events during the study period showed significant wave heights above 5 m and it is found that the cyclogenetic pattern between latitudes 31.5 $^\circ$ and 34 $^\circ$ S is the most favourable for the development of high waves.

This work aims at verifying and comparing the behaviour of wave parameters near two coastal regions of Brazil using the model SWAN with boundary data provided by the ocean wave model WAVEWATCH III and by ENVISAT. This analysis was conducted in the southern and northeastern coastal regions of Brazil during events with predominant swell.

The reason to use events which swell waves were prevalent is because of the fact that the ENVISAT satellite measures the directional spectrum of long waves only. For the selection of events, a sweep in the WAVEWATCH III data (`ftp://polar.ncep.noaa.gov/pub/history/waves`) were performed in the period of the years 2002-2010 with events where the wavelength ranged in the interval $(100, 400)$ m which is equivalent to wave periods in about $(8, 16)$ s. Furthermore, we also required average significant wave heights to be greater than 2 m, in the selection.

5.2 Study area

5.2.1 South region of Brazil

The coast of Rio Grande do Sul state is characterised by a broad coastal plain of approximately 615 km featuring a NE-SW orientation (DILLENBURG et al., 2000). It consists of unconsolidated quaternary deposits that do not have modern sands contributions from the continent. The continental shelf has 150-200 km wide, with maximum depths ranging from 100 to 140 m, and gentle slopes of 0.03 ° to 0.08 °. The shoreface is wide and shallow with an outer boundary at a depth of 10-15 m, with a predominance of sandy sediments (Toldo Jr et al., 2006). Because it is an open coast without a natural hedge, this is vulnerable to the action of waves, characterised by dominant swell generated in the South Atlantic and also by sea waves.

Cuchiara et al. (2009) obtained a characterisation of the wave climate based on a thorough review of existing field data and numerical modelling experiments. They found that wave regime in southern Brazilian shelf is characterised by waves of predominant directions of 100 ° and 160 ° with average significant wave heights ranging from 1 to 1.50m. The wave period varies between 6 and 14 s with a predominance of 8 s for sea and 12 s for swell.

5.2.2 Northeast region of Brazil

The Northeast region was chosen because part of its coast is susceptible to swell events originated in distant areas of the North Atlantic.

Sedimentation is influenced by semi-arid climate in the coastal zone, resulting in a reduced contribution to the river shore, with a small amount of silty-clay material transported (Maia, 1998). The current sedimentation is mainly carbonate with no hermatypic coral (CARANNANTE et al., 1988).

According to Innocentini et al. (2001), the incident waves in the northeastern region are formed by trade winds and feature height below 1-1.5 m in open sea. Occasionally waves with periods between 15 and 20 s may rise coming from the North Atlantic storms. This region consists of local waves originated by the trade winds and swell generated by tropical cyclones in both hemispheres (INNOCENTINI et al., 2005).

5.3 Materials and methods

5.3.1 Model description

SWAN (Simulating Waves Nearshore) is a wave model of third generation for realistic estimates of wave parameters in coastal areas, lakes and estuaries from wind data, bathymetry and currents (BOOIJ; RIS; HOLTHUIJSEN, 1999; RIS; HOLTHUIJSEN; BOOIJ, 1999). The model is based on the balance wave action equation. This equation includes source terms for wind input, nonlinear interactions, white-capping, friction with the bottom and wave breaking. In this study, we used the 41.01 version of the SWAN model and two grids; one in the south and another in the northeast of Brazil.

The grid used in the southern region is curvilinear and has 275200 (800×344) cells with a higher resolution of 0.5 km off the coast and lower resolution of 1.5 km in deep water, rotated at 45° (Figure 5.1). The domain area is approximately 250000 km^2, covering the entire coast of the state of Rio Grande do Sul, part of the state of Santa Catarina and part of Uruguay. The bathymetry used for this grid was a combination of ETOPO1 model data with resolution of $1' \times 1'$ (AMANTE; EAKINS, 2009) with nautical charts available from DHN / CHM (Brazil Navy) (`https://www.mar.mil.br/dhn/chm/box-cartas-nauticas/cartas.html`) which was obtained by using model data and the Oceanographic Observation Network (REMO).

In the northeast, the grid is also curvilinear with higher resolution near the coast and lower in deep water, having 524880 (1215×432) cells. This grid involves the entire coasts of the states of Piauí and Ceará, and part of the states of Maranhão and Rio Grande do Norte (Figure 5.1). The bathymetry for this grid is composed only of data of the General Bathymetric Chart of the Oceans (GEBCO) with resolution of $30'' \times 30''$.

The model was executed in non stationary mode, with 5 minute time step and wind data input every 3 hours.

5.3.2 Satellite data

The ENVISAT satellite was launched in March 2002 by the European Space Agency with instruments that could substitute the data sent by the satellite ERS, his predecessor. The main objective of ENVISAT data was to provide atmosphere, ocean, land and ice data, aimed at monitoring global warming, the degree of air pollution and natural disaster risks. ENVISAT had ten instruments on board, divided between optical sensors and active sensors, with its main optical sensor being MERIS (Medium Resolution Imaging Spectrometer) and its main asset, the ASAR sensor. The ENVISAT mission ended on 08 April 2012, after the unexpected loss of

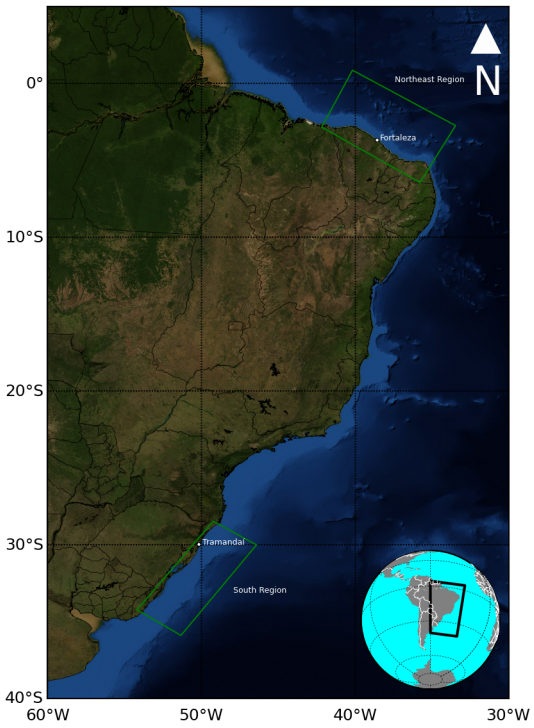

Figure 5.1: Study area with two grids in the southern and northeastern regions. The dots show the cities of reference for this study.

contact with the satellite.

The ASAR sensor was an enhanced version of the SAR instrument that was already in operation on board satellites ERS-1 and ERS-2: The ASAR had a 10 m long antenna, and operated in five different modes: image mode, mode alternating polarisation wide band mode, monitor mode, and global wave mode. These modes had resolutions ranging from 25 km to 1 km, specially developed to observe continental areas, ocean areas and polar ice caps. The sensor in wave mode generated small images, called "imagettes"of the surface of the sea with 5 km x 5-10 km, similar to ERS SAR, over 100 km of the satellite orbit. These small images were processed to derive the wave spectrum of the sea surface and hence the wavelength, period, height and direction of the waves. The processing of Level 2 data used an algorithm developed and implemented by IFREMER / CERSAT (JOHNSEN et al., 2006).

5.3.3 Boundary conditions and Statistics indices

For the boundary conditions we used data from the third generation wave model WAVEWATCH III (or simply WW3) (TOLMAN, 1999) developed by NOAA / NCEP and data obtained by the ENVISAT satellite, through the ASAR sensor.

The WW3 wave model solves the spectral action energy conservation equation. The physical model includes generation, dissipation due to breaking waves in the bottom, refraction, advection and nonlinear interactions. Our implementation includes the globe with domain ($78\,^{\circ}S - 78\,^{\circ}N$) and spatial resolution of $1\,^{\circ} \times 1.25\,^{\circ}$ in latitude and longitude respectively. Temporal resolution was 3 hours and wind fields, obtained from the Global Data Assimilation Scheme (GDAS), were input in the model in 3 hour intervals. This model outputs the wind speed and direction, as well as the integrated spectral parameters, such as significant wave height H_s, peak period T_p and the mean direction at the peak period D_p.

Data from WAVEWATCH III were nested in SWAN as boundary conditions. The wind components U and V, from the WAVEWATCH III for every 3 hours, were adjusted to the computational grid using a linear interpolation based on the Delaunay triangulation, and then these were smoothed on the model grid (GUIMARÃES; FARINA; Toldo Jr., 2014). With regard to satellite data, the closest measure to the edge parallel to the coast were used. The initial conditions were defined based on a non-stationary JONSWAP spectrum distribution obtained through the wave parameters H_s, T_p and D_p and directional spreading.

To ascertain the quality of results from the two simulations, various statistical parameters as root mean square error (*RMSE*) Eq.(5.1), scattering index (*SI*) Eq.(5.2), bias Eq.(5.3), bias mean square slope (*SS*) Eq.(5.4) and the Pearson correlation coefficient (R) Eq.(5.5) were used and given by

$$RMSE = \sqrt{\frac{1}{n}\sum_{i=1}^{n}(M-S)^2}, \tag{5.1}$$

$$SI = \frac{\sqrt{\frac{1}{n}\sum_{i=1}^{n}(M-S)^2}}{\bar{S}}, \tag{5.2}$$

$$Bias = \bar{M} - \bar{S}, \tag{5.3}$$

$$SS = \sqrt{\frac{\sum_{i=1}^{n}(M)^2}{\sum_{i=1}^{n}(S)^2}} \tag{5.4}$$

$$R = \frac{\sum_{i=1}^{n}(M_i - \bar{M})(S_i - \bar{S})}{\sqrt{\sum_{i=1}^{n}(M_i - \bar{M})^2} \cdot \sqrt{\sum_{i=1}^{n}(S_i - \bar{S})^2}} \tag{5.5}$$

where M refers the model results and S the satellite measurements with $\bar{M}$ and $\bar{S}$ representing their mean values and n is the number of data points.

5.4 Results and discussion

We studied a total of six events in the period 2002 and 2009; three in the South region and three in the Northeast. These events represent cases where the swell is dominant. Table

5.1 presents these six events separated by region and with the start and end date. These dates represent the period when the swell prevailed. The maximum significant wave height $H_{s_{max}}$, mean significant wave height $\bar{H_s}$, mean peak period $\bar{T_p}$, period of the most frequent peak waves $T_{p_{freq}}$ and direction of most frequent peak waves $D_{p_{freq}}$ for the regions of the two grids are also displayed in the table 5.2.

These parameters are presented for WW3 data (boundary conditions obtained by WW3) and satellite data (boundary conditions obtained by ENVISAT data).

Table 5.1: Studied events.

South Region		
Events	Start date	End date
E01S	19 August 2004	31 August 2004
E02S	27 May 2007	08 June 2007
E03S	24 July 2007	02 August 2007
Northeast Region		
E01N	01 March 2006	08 March 2006
E02N	06 December 2006	22 December 2006
E03N	17 January 2009	29 January 2009

Table 5.2: Wave parameters for each event and for each type of boundary conditions (WW3 and Satellite).

	WW3					Satellite				
South Region										
Events	$H_{s_{max}}$ (m)	$\bar{H_s}$ (m)	$\bar{T_p}$ (s)	$T_{p_{freq}}$	$D_{p_{freq}}$	$H_{s_{max}}$ (m)	$\bar{H_s}$ (m)	$\bar{T_p}$ (s)	$T_{p_{freq}}$	$D_{p_{freq}}$
E01S	6,057	1,9582	8,1981	(8-10)	S	6,076	2,0238	9,7834	(12-14)	S
E02S	6,681	2,1613	7,7935	(8-10)	S	6,3	2,0475	8,395	(10-12)	S
E03S	6,607	2,0575	7,7678	(6-8)	S	5,607	2,0531	9,1992	(12-14)	S
Northeast Region										
E01N	4,569	1,752	8,5116	(8-10)	NE	3,873	1,8781	11,6034	(14-16)	NE
E02N	4,225	1,8596	8,4988	(8-10)	NNE	3,6	1,9409	11,7549	(14-16)	NNE
E03N	4,295	2,1448	9,4066	(8-10)	NNE	3,924	2,2211	12,6664	(12-14)	NNE

Comparisons between the two simulations will be separated according to their regions in the next two subsections.

5.4.1 South region

According to table 5.2 events in the southern region had a mean significant wave height of approximately 2 m, with both types of boundary conditions. The mean peak period was approximately 8 s for WW3 boundary data and 9 s for satellite boundary data. In the three events studied, two lasted 12 days (E01 and E02) and another 9 days (E03), all of which occurred during the fall/winter in the Southern Hemisphere.

To compare the two simulations and also to analyse the behaviour of wave parameters as time series we considered two points within the computational domain at *n* different times; one located in shallow water (30 ° S, 50.05999 ° W with ≈20 m depth), near the city of Tramandaí, and other in deep water (30.8679 ° S, 48.9691 ° W, with >2000 m depth). The results are shown in table 5.3. The results show correlation between the two simulations for each of the events. H_s, T_p and D_p correspond to of all grid points, $H_{s_{sw}}$, $T_{p_{sw}}$ and $D_{p_{sw}}$ are the variables in the shallow points and $H_{s_{dw}}$, $T_{p_{dw}}$ and $D_{p_{dw}}$ denote the points in deep water. R is the Pearson correlation coefficient, and R^2 the coefficient of determination. The RMSE values (*RMSE*), scattering index (*SI*), mean square slope (*SS*) and (*Bias*) are also presented.

Table 5.3: Statistical parameters for the three events in the southern region for *n* different times at two locations; shallow water (*sw*) and deep water (*dw*). R and R^2 are the Pearson correlation coefficient and the coefficient of determination.

South Region							
Event E01S	n	*RMSE*	*SI*	*SS*	*Bias*	*R*	R^2
H_s	79863705	0,3631	0,1824	0,9951	-0,0536	0,957	0,915849
T_p	79863705	3,2091	0,3583	0,8395	-1,2958	0,839	0,703921
D_p	79863705	24,2798	0,1434	0,9932	-1,4525	0,953	0,9082
$H_{s_{sw}}$	289	0,2487	0,191	0,9747	-0,0635	0,901	0,8118
$T_{p_{sw}}$	289	3,7019	0,3884	0,8368	-1,8713	0,669	0,4476
$D_{p_{sw}}$	289	10,926	0,0733	1,0038	0,3114	0,952	0,9063
$H_{s_{dw}}$	289	0,5573	0,2059	1,0026	-0,1101	0,886	0,785
$T_{p_{dw}}$	289	4,549	0,4267	0,8065	-2,6052	0,201	0,0404
$D_{p_{dw}}$	289	45,3781	0,2505	0,9573	-11,9377	0,474	0,2247
Event E02S	n	*RMSE*	*SI*	*SS*	*Bias*	*R*	R^2
H_s	79863705	0,4	0,1902	1,0751	0,0931	0,96	0,9216
T_p	79863705	1,9513	0,2412	0,9176	-0,4917	0,908	0,8245
D_p	79863705	22,3911	0,1213	1,0039	1,4938	0,963	0,9274
$H_{s_{sw}}$	289	0,2606	0,2078	1,095	0,0707	0,92	0,8464
$T_{p_{sw}}$	289	3,0455	0,3663	0,9036	-0,749	0,658	0,433
$D_{p_{sw}}$	289	12,4228	0,0744	1,0071	1,0381	0,888	0,7885
$H_{s_{dw}}$	289	0,5354	0,1789	1,05	0,1	0,874	0,7639
$T_{p_{dw}}$	289	2,491	0,2566	0,8905	-1,1177	0,501	0,251
$D_{p_{dw}}$	289	23,054	0,1169	1,002	1,7993	0,768	0,5898
Event E03S	n	*RMSE*	*SI*	*SS*	*Bias*	*R*	R^2
H_s	59966865	0,4049	0,197	1,031	0,0036	0,953	0,9082
T_p	59966865	2,5686	0,3039	0,826	-1,17	0,902	0,8136
D_p	59966865	23,0244	0,1301	1,011	1,931	0,962	0,9254
$H_{s_{sw}}$	217	0,3066	0,2251	0,9877	-0,0466	0,834	0,6956
$T_{p_{sw}}$	217	2,6785	0,3301	0,826	-1,4085	0,867	0,7517
$D_{p_{sw}}$	217	24,2681	0,158	1,0347	5,7143	0,832	0,6922
$H_{s_{dw}}$	217	0,5509	0,1818	1,0136	-0,0299	0,857	0,7344
$T_{p_{dw}}$	217	2,8195	0,2786	0,8309	-1,7351	0,713	0,5084
$D_{p_{dw}}$	217	25,8318	0,1315	1,0064	2,0276	0,789	0,6225

We observe in table 5.3 that generally there is fair correlation between the two simulations for all parameters of waves studied, in shallow and deep water. Exceptions to this are observed for $D_{p_{dw}}$ and $T_{p_{dw}}$ for the event E01, where the coefficients of Pearson are well below the ones found for other variables and events.

In all events, larger values of the scattering index are observed for the peak period. Regarding the *SS* and bias results, we see that the peak period is underestimated by the WW3 boundary data simulation in all events, both in shallow and deep water. This corroborate with Poças et al. (2010) conclusions in which WW3 model data tend to be underestimated compared to ASAR wave data. We also observe that the bias in the significant wave height are very small in all cases and much less than those shown for the peak direction, although in the former case

there is not a consistent tendency detected.

We show in figures 5.2-5.4 the significant wave height and peak period in selected times where the bias reached its larger absolute values during each event. It can bee seen that H_s is generally overestimated by the WW3 boundary data simulation in all three cases with the exception with a small region in the southwest of the domain where a negative bias occurred. Regarding the peak period we have three remarks. First, only in the event E02 (figure 5.3) the bias is prominently negative, meaning larger T_p with the satellite boundary data. Second, in the event E01 (figure 5.2), the region where the bias is negative corresponds very closely to the H_s negative bias. This confirms an observation, supported by simulations of other times of the events, that negative bias in H_s is accompanied by negative bias in T_p. This suggests that the wave height is typically underestimated by the model when it does not *detect* longer waves. Finally, a narrow region delimited by the south of Patos lagoon and extending southwards, where the bias is noticeable larger and positive, is seen in figures 5.2 and 5.3. This can be identified roughly as the boundary of the area most affected by high waves generated by extra-tropical cyclones in the South Atlantic.

5.4.2 Northeast region

The data in table 5.2 show that the events studied in the Northeast region are not as energetic as the ones we considered in the South region. Nevertheless, these events presented longer waves and thus, they fit for a comparison using ASAR data. The mean significant wave height was slightly underestimated by the simulation with WW3 data, while the maximum significant wave height was overestimated by it.

The first event (E01N) lasted 7 days, the second (E02N), 16 days and the third (E03N) 12 days. All these took place during spring or summer in the Southern Hemisphere.

In this region we also selected two points within the computational domain for a local analysis. As the previous case, these points are located in shallow water (3.618420 $^\circ$ S, 38 $^\circ$ W with $\approx$20 m depth), near the city of Fortaleza, and in deep water (2.1213 $^\circ$ S, 36.7121 $^\circ$ W with $>$2000 m depth).

As shown in table 5.4, there is a overall significant correlation, with exceptions, between the two simulations in all wave parameters. The correlation is lowest for T_p, mainly in the E03N event where the bias is negative. This event also had the lowest correlation values for H_s.

As observed in the southern region, the largest discrepancy between the simulated values occurs for T_p at all events, both for shallow and deep water environments. We notice also that on average the simulation with WW3 boundary data underestimated H_s and T_p in all events.

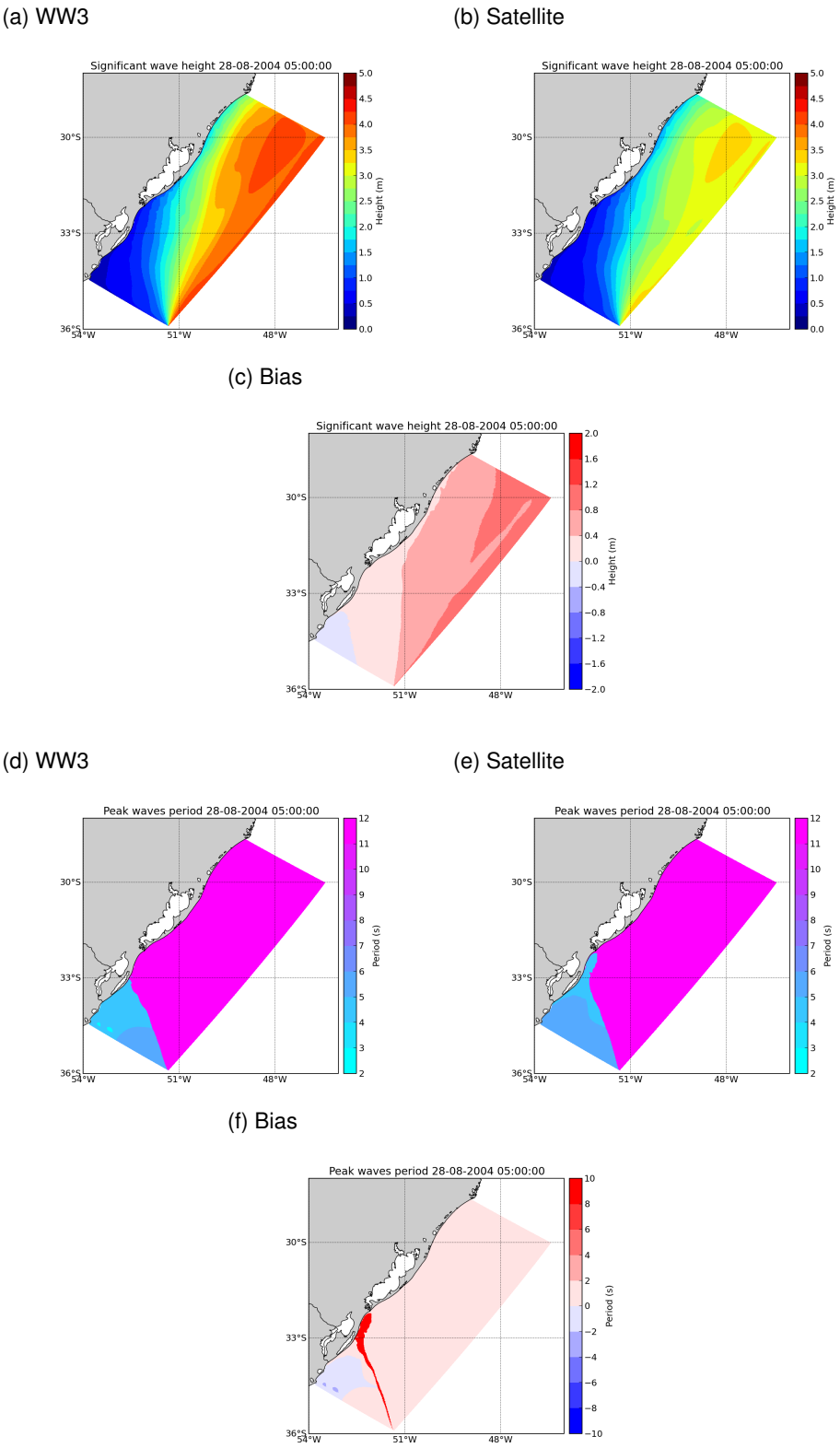

Figure 5.2: Map wave field for H_s and T_p during event E01, where (a)(d) WW3, (b)(e) Satellite and (c)(f) Bias.

In figures 5.5-5.7, the wave field in terms of H_s and T_p are represented for selected times when the absolute value of bias was largest in each of the events. The first two events share the what is a overestimation of H_s by the simulation with WW3 data and in turn underestimate T_p, particularly in E02N. Although, the bias in H_s is also positive in E03N, the peak period is not

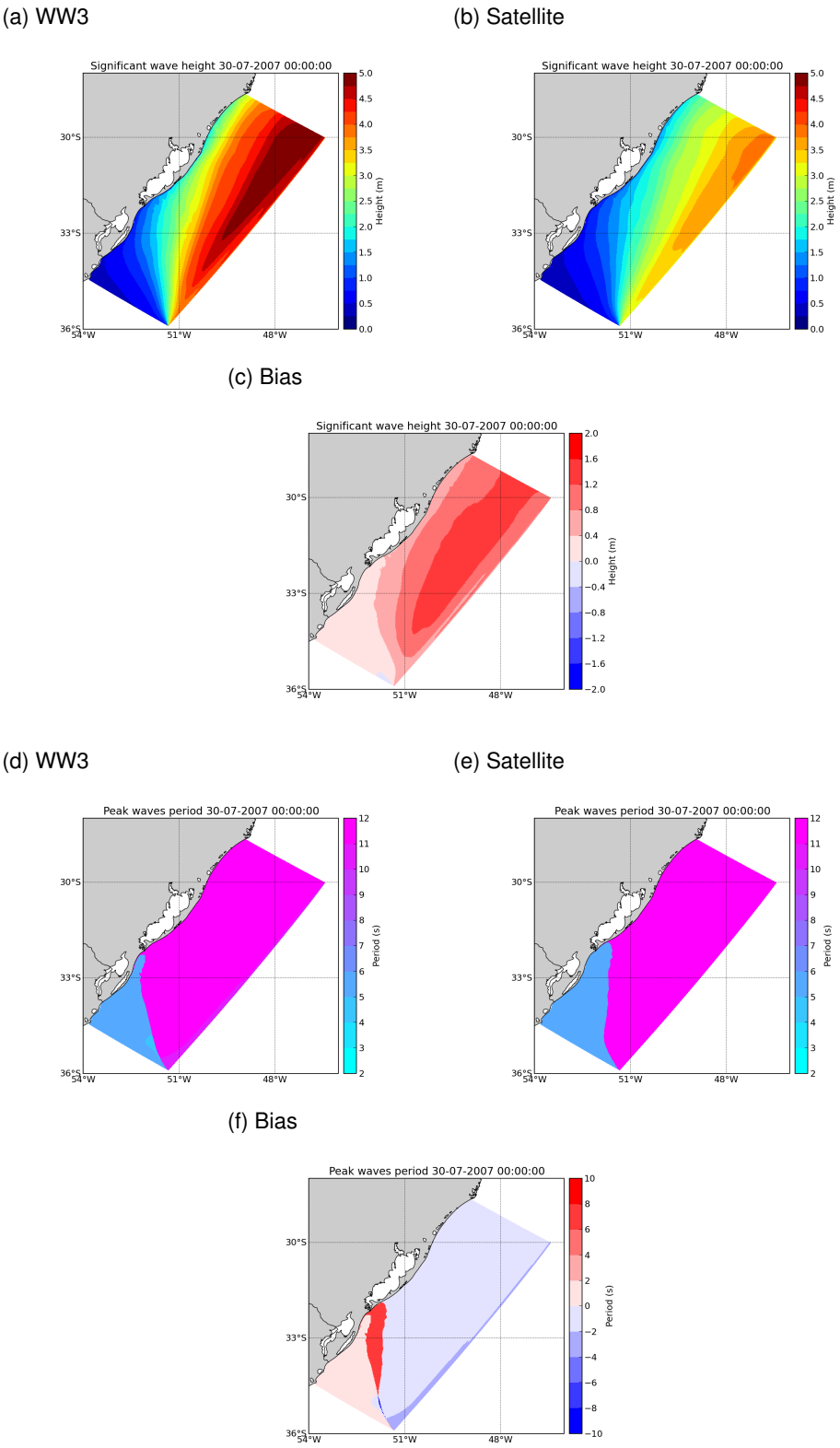

Figure 5.3: Map wave field for H_s and T_p during event E02, where (a)(d) WW3, (b)(e) Satellite and (c)(f) Bias.

underestimated by the simulation with WW3 data.

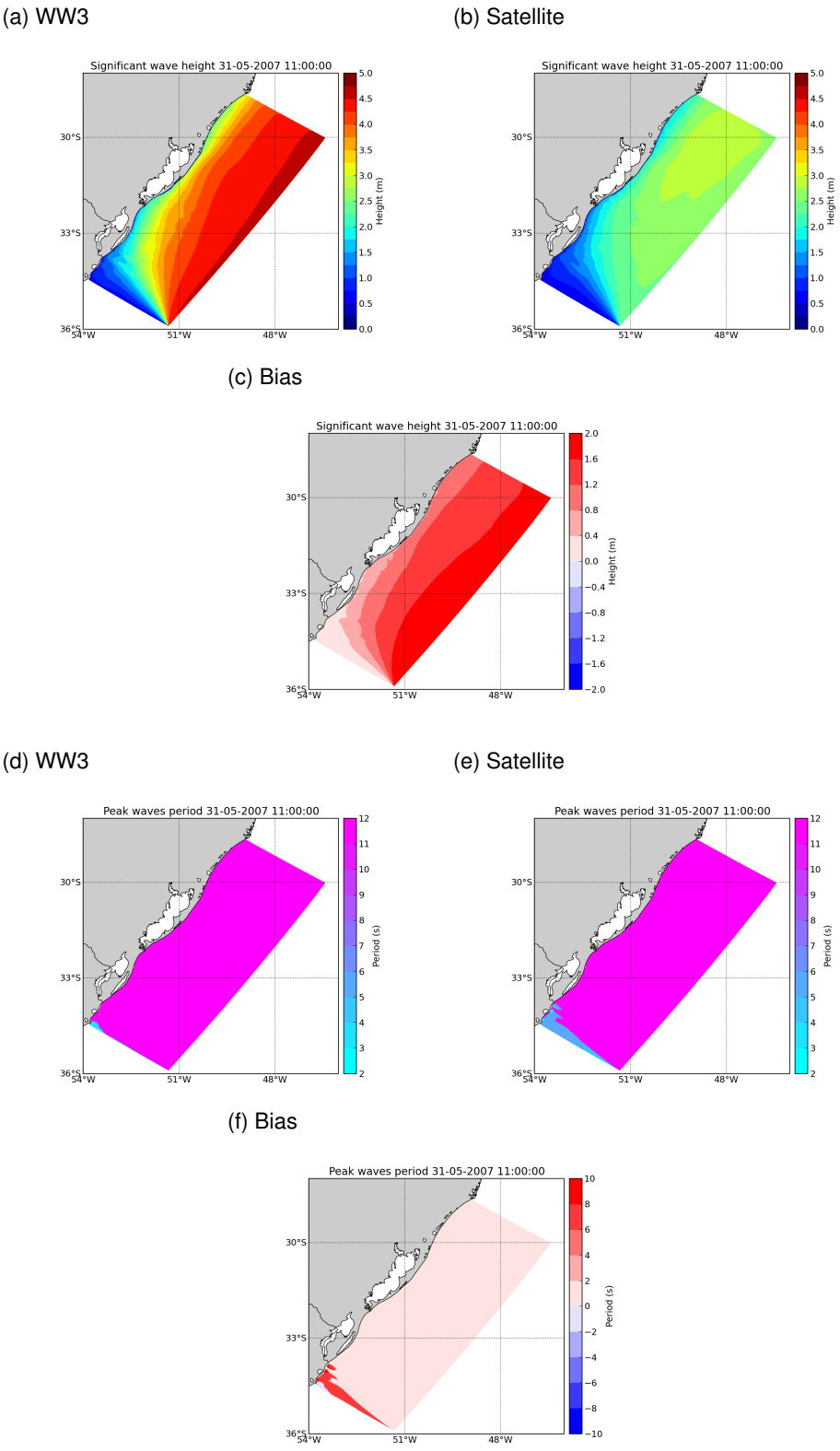

Figure 5.4: Map wave field for H_s and T_p during event E03, where (a)(d) WW3, (b)(e) Satellite and (c)(f) Bias.

5.5 Conclusion

In this paper we present a study of six events, three located in the south region and another 3 in the Northeast region of Brazil between 2002 and 2009, prioritising events where the swell

was dominant. These events were selected based on the period range captured by the satellite ENVISAT to propitiate a more realistic comparison. WW3 and satellite data were used as boundary conditions in the simulations with SWAN. The two simulations were compared in time and space and in selected points located in shallow and deep water for each event.

The results show that there was an overall correlation shown by the Pearson coefficient between the two simulations studied, particularly in the South region. As a general conclusion, we point out that the T_p has the lowest values for the coefficient of Pearson and also negative bias, meaning that the simulation with WW3 boundary data underestimated this variable.

We noticed also that H_s presented a very small bias. However the significant wave height was consistently higher in the simulation with the WW3 data in the critical times where the events presented largest absolute bias. Moreover, in the Northeast region, where the swell was more dominant, we found that the maximum significant wave height was higher for the simulations with WW3 data.

Acknowledgements

The first author acknowledges financial support by CAPES, Brazil, through the Project Edital Capes Ciências do Mar 09/2009. The second author has done part of the research on this article while a member of the EU Project FP7-295217, HPC-GA. His research was supported by

Table 5.4: Statistics parameter values for the Northeast region. *RMSE* is the root mean square error, *SI* scattering index, *SS* a mean square slope and *Bias*.

Northeast Region							
Event E01N	n	*RMSE*	*SI*	*SS*	*Bias*	*R*	R^2
H_s	88983232	0,2733	0,1507	0,9399	-0,0686	0,969	0,939
T_p	88983232	3,3962	0,3417	0,7299	-1,6819	0,913	0,8336
D_p	88983232	10,1017	0,2237	0,9717	-0,5593	0,941	0,8855
$H_{s_{sw}}$	169	0,3299	0,2057	0,8999	-0,1661	0,597	0,3564
$T_{p_{sw}}$	169	4,5175	0,412	0,737	-3,4668	0,587	0,3446
$D_{p_{sw}}$	169	20,8261	0,3897	0,8717	-9,7633	0,553	0,3058
$H_{s_{dw}}$	169	0,3934	0,1561	0,9976	-0,0302	0,622	0,3869
$T_{p_{dw}}$	169	4,4603	0,3878	0,7446	-3,4976	0,341	0,1163
$D_{p_{dw}}$	169	7,4182	0,1717	0,9807	-0,7692	0,956	0,9139
Event E02N							
H_s	202713280	0,2213	0,1165	0,9648	-0,0442	0,979	0,9584
T_p	202713280	3,5991	0,3601	0,7132	-1,7713	0,911	0,8299
D_p	202713280	13,9198	0,2719	0,9644	-1,3437	0,919	0,8446
$H_{s_{sw}}$	385	0,2603	0,1485	0,9499	-0,1005	0,759	0,5761
$T_{p_{sw}}$	385	5,2882	0,5114	0,6985	-3,7525	0,519	0,2694
$D_{p_{sw}}$	385	20,3923	0,2982	0,9534	-6,2597	0,585	0,3422
$H_{s_{dw}}$	385	0,317	0,1314	0,9944	-0,03	0,735	0,5402
$T_{p_{dw}}$	385	4,8922	0,421	0,709	-4,0102	0,486	0,2362
$D_{p_{dw}}$	385	14,013	0,3328	0,9464	-2,1299	0,912	0,8317
Event E03N							
H_s	152166592	0,2487	0,114	0,9671	-0,0415	0,979	0,9584
T_p	152166592	2,8299	0,2593	0,7397	-1,7733	0,97	0,9409
D_p	152166592	5,614	0,162	1,0134	0,2624	0,962	0,9254
$H_{s_{sw}}$	289	0,2922	0,1481	0,9364	-0,1265	0,229	0,0524
$T_{p_{sw}}$	289	3,7789	0,3371	0,7395	-3,3641	-0,261	0,0681
$D_{p_{sw}}$	289	3,9019	0,0843	0,9796	-0,8997	0,977	0,9545
$H_{s_{dw}}$	289	0,3849	0,1408	1,0046	0,0146	0,303	0,0918
$T_{p_{dw}}$	289	3,7836	0,338	0,7395	-3,3567	-0,285	0,0812
$D_{p_{dw}}$	289	1,1765	0,0362	1	0	0,987	0,9742

(a) WW3 (b) Satellite

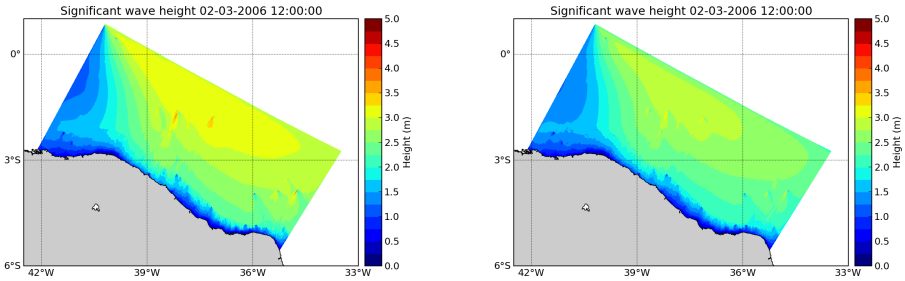

(c) Bias

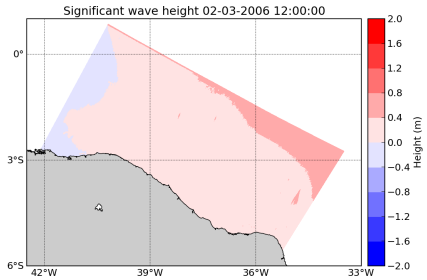

(d) WW3 (e) Satellite

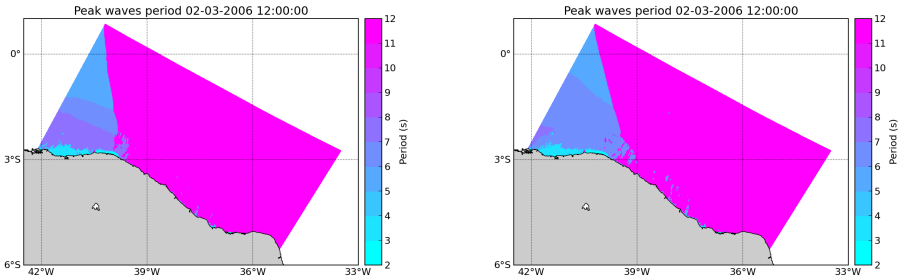

(f) Bias

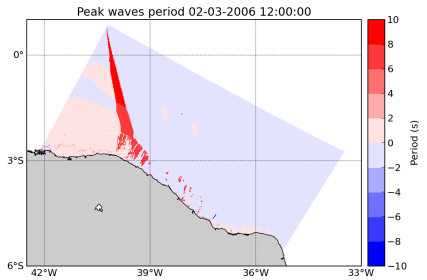

Figure 5.5: Map wave field for H_s and T_p during event E01N, where (a)(d) WW3, (b)(e) Satellite and (c)(f) Bias.

the Basque Government through the BERC 2014-2017 program an by the Spanish Ministry of Economy and Competitiveness MINECO: BCAM Severo Uchoa excellence accreditation SEV-2013-0323.

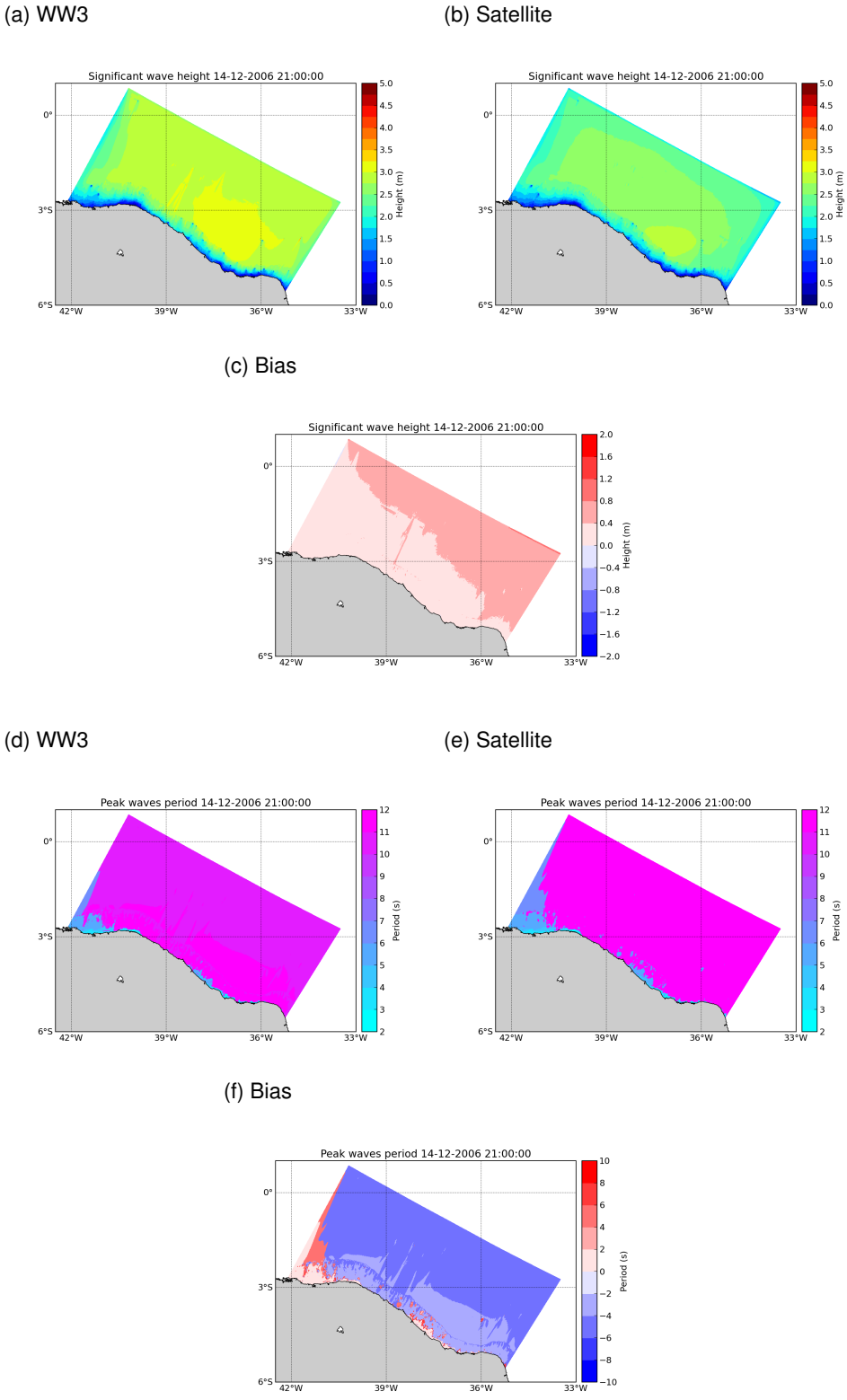

Figure 5.6: Map wave field for H_s and T_p during event E02N, where (a)(d) WW3, (b)(e) Satellite and (c)(f) Bias.

(a) WW3

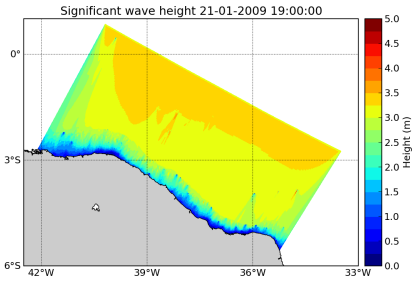

(b) Satellite

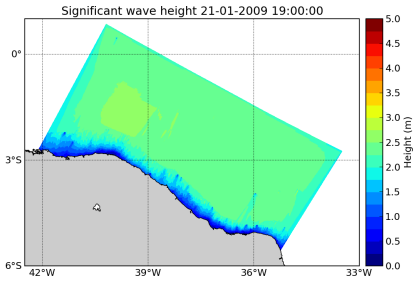

(c) Bias

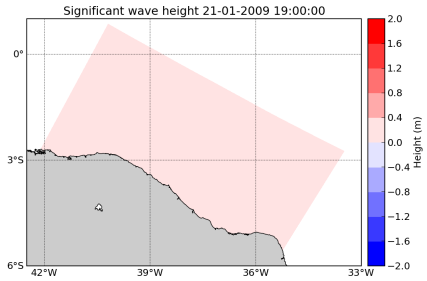

(d) WW3

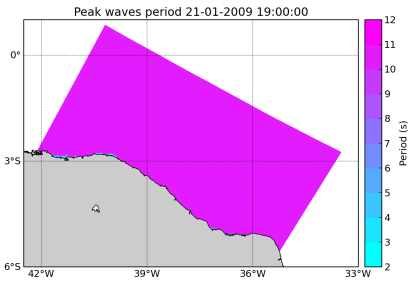

(e) Satellite

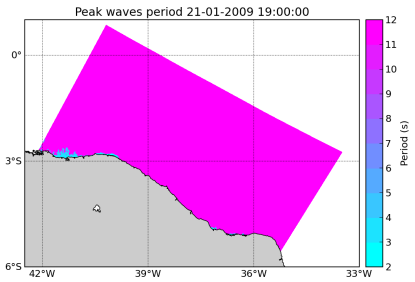

(f) Bias

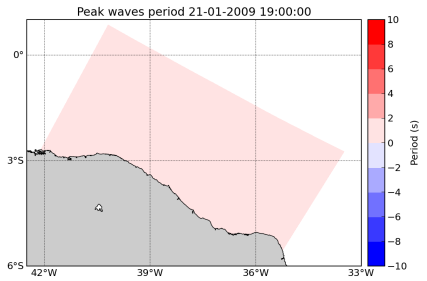

Figure 5.7: Map wave field for H_s and T_p during event E03N, where (a)(d) WW3, (b)(e) Satellite and (c)(f) Bias.

References

AMANTE, C.; EAKINS, B. ETOPO1 1 Arc-Minute Global Relief Model: Procedures, Data Sources and Analysis. *NOAA Technical Memorandum NESDIS NGDC-24*, Boulder, Colorado, 2009.

BOOIJ, N.; RIS, R. C.; HOLTHUIJSEN, L. H. A third-generation wave model for coastal regions: 1. Model description and validation. *Journal of Geophysical Research*, v. 104, n. C4, p. 7649, 1999. ISSN 0148-0227. Disponível em: <http://doi.wiley.com/10.1029/98JC02622>.

CARANNANTE, G. et al. Carbonate lithofacies as paleolatitude indicators: problems and limitations. *Sedimentary Geology*, v. 60, n. 1-4, p. 333–346, nov. 1988. ISSN 00370738. Disponível em: <http://linkinghub.elsevier.com/retrieve/pii/0037073888901285>.

CUCHIARA, D. et al. Determination of the wave climate for the southern Brazilian shelf. *Continental Shelf Research*, v. 29, n. 3, p. 545–555, mar. 2009. ISSN 02784343. Disponível em: <http://linkinghub.elsevier.com/retrieve/pii/S0278434308003622>.

DILLENBURG, S. R. et al. Influence of antecedent topography on coastal evolution as tested by the shoreface translation-barrier model (STM). *Journal Of Coastal Research*, v. 16, n. 1, p. 71–81, 2000. ISSN 0749-0208. Disponível em: <http://www.jstor.org/stable/4300012>.

GREENSLADE, D. The assimilation of ERS-2 significant wave height data in the Australian region. *Journal of Marine Systems*, v. 28, n. 1-2, p. 141–160, fev. 2001. ISSN 09247963. Disponível em: <http://linkinghub.elsevier.com/retrieve/pii/S0924796301000057>.

GUIMARÃES, P. V.; FARINA, L.; Toldo Jr., E. E. Analysis of extreme wave events on the southern coast of Brazil. *Natural Hazards and Earth System Science*, v. 14, n. 12, p. 3195–3205, dez. 2014. ISSN 1684-9981. Disponível em: <www.nat-hazards-earth-syst-sci.net/14/3195/2014/ http://www.nat-hazards-earth-syst-sci.net/14/3195/2014/>.

INNOCENTINI, V. et al. Ocorrência de vagas no Arquipélago de São Pedro e São Paulo: Caso 24 de Outubro de 1999. *Revista Brasileira de Meteorologia*, v. 16, n. 2, p. 177–186, 2001.

INNOCENTINI, V. et al. A AGITAÇÃO MARÍTIMA NO LITORAL NORDESTE DO BRASIL ASSOCIADA AOS DISTÚRBIOS AFRICANOS DE LESTE. *Revista Brasileira de Meteorologia*, v. 20, p. 367–374, 2005.

JOHNSEN, H. et al. Envisat asar wave mode products - quality assessment and algorithm upgrade. In: ESA (Ed.). *SEASAR 2006, Advances in SAR Oceanography from ENVISAT and ERS missions*. Frascati, Italy: [s.n.], 2006.

LI, J.-G.; HOLT, M. Comparison of Envisat ASAR Ocean Wave Spectra with Buoy and Altimeter Data via a Wave Model. *Journal of Atmospheric and Oceanic Technology*, v. 26, n. 3, p. 593–614, mar. 2009. ISSN 0739-0572. Disponível em: <http://journals.ametsoc.org/doi/abs/10.1175/2008JTECHO529.1>.

LI, J.-G.; SAULTER, A. Assessment of the updated Envisat ASAR ocean surface wave spectra with buoy and altimeter data. *Remote Sensing of Environment*, Elsevier B.V., v. 126, p. 72–83, nov. 2012. ISSN 00344257. Disponível em: <http://linkinghub.elsevier.com/retrieve/pii/S0034425712003318>.

POÇAS, J. S. et al. Análise comparativa dos espectros de ondas observados ao largo de Santa Catarina e de Rio Grande por ondógrafos, radar de abertura sintética e derivados de modelo. In: *4° Seminário e Workshop em Engenharia Oceânica*. Rio Grande - RS: [s.n.], 2010. p. 1–11.

REN, Q. et al. Comparison and analysis of Envisat ASAR ocean wave spectra with buoy data in the northern Pacific Ocean. *Chinese Journal of Oceanology and Limnology*, v. 29, n. 1, p. 10–17, jan. 2011. ISSN 0254-4059. Disponível em: <http://link.springer.com/10.1007/s00343-011-9926-8>.

RIS, R. C.; HOLTHUIJSEN, L. H.; BOOIJ, N. A third-generation wave model for coastal regions: 2. Verification. *Journal of Geophysical Research*, v. 104, n. C4, p. 7667, 1999. ISSN 0148-0227. Disponível em: <http://doi.wiley.com/10.1029/1998JC900123>.

ROCHA, R. P. da; SUGAHARA, S.; SILVEIRA, R. B. da. Sea Waves Generated by Extratropical Cyclones in the South Atlantic Ocean: Hindcast and Validation against Altimeter Data. *Weather and Forecasting*, v. 19, n. 2, p. 398–410, abr. 2004. ISSN 0882-8156. Disponível em: <http://journals.ametsoc.org/doi/abs/10.1175/1520-0434(2004)019<0398:SWGBEC>2.0.CO;2>.

Toldo Jr, E. E. et al. Coastal Dunes and Shoreface Width as a Function of Longshore Transport . *Journal of Coastal Research*, SI 39, n. 39, p. 390–394, 2006. Disponível em: <http://www.jstor.org/stable/25741602>.

TOLMAN, H. L. *User manual and system documentation of WAVEWATCH-III version 1.18*. Washington, DC, 1999. 110 p.

6 Conclusão

Este trabalho usou o modelo WAVEWATCH III (WW3) como ferramenta para a obtenção de aspectos importantes em uma determinada região do Atlântico Sul que é vulnerável ao impacto de eventos extremos entre 2001 a 2009. O modelo WW3 também foi utilizado para uma comparação global com dados do satélite ENVISAT da Agência Espacial Europeia (ESA) através do sensor ASAR para o ano de 2007. Os dados do modelo e do satélite também foram utilizados como entrada para o modelo SWAN, que foi utilizado em eventos em que as ondas de swell eram predominantes. Utilizando os dados das componentes U e V do vento provenientes do modelo WW3 foram calculadas as trajetórias dos ciclones extratropicais entre 2001 a 2009. Estas foram classificadas em três padrões, o Padrão III é o mais comum (41,4%), com uma maior incidência de eventos que aparecem em maio. A influência destes padrões foi analisada para três cidades da região Sul, Garopaba (SC), Tramandaí (RS) e Rio Grande (RS). Verificou-se que os ventos dominantes dos padrões I, II e III foram, respectivamente, NE, SW e SW em todos os três locais. Os maiores valores de altura média e altura máxima de onda estão associados aos padrões II e III, que são os mais erosivos e os que geram as maiores elevações no nível do mar, respectivamente. Os maiores valores de altura de onda estão associados com os padrões II e III (87,5%), especialmente o último. Foram encontrados um total de 28 eventos, onde foi observada uma boa correlação global entre os dados de altura de onda significativa e velocidade do vento. O evento de número 3 apresentou a ocorrência simultânea de dois ciclones causando danos à linha de costa em várias cidades. Os valores de altura de onda e intensidade do vento deste evento se mostraram superiores aos demais. Durante este evento Garopaba apresentou valores de altura e intensidade do vento mais elevados. O evento ocorrido em Maio de 2001 produziu altura significativa máxima da onda que superou em cerca de 10% todos os outros eventos (com exceção do evento 28) em todos os 11 anos analisados.

Dados do satélite ENVISAT, obtidos por um sensor ASAR, foram comparados com os dados do modelo WW3 para o ano de 2007. Utilizando parâmetros estatísticos como viés e índice de espalhamento a altura de swell foi analisada. Neste trabalho, foi introduzido um algoritmo para representar dados irregulares de onda do satélite em uma malha uniforme. Este procedimento também permite a comparação entre dados de satélite e modelo no mesmo ponto no espaço e no tempo. Este algoritmo é uma grande contribuição para a tese em geral. As maiores

alturas foram observadas em altas latitudes (60 ° N e 60 ° S) para ambos os hemisférios. O HS apresentou os maiores valores de altura de swell, principalmente pelo fato do período analisado compreender outono e inverno neste hemisfério. Analisando os valores de viés constatou-se que as maiores variações ocorrem em altas latitudes, predominando valores negativos. Sendo assim, na altura de swell ocorreu uma maior subestimação dos valores do modelo em relação aos valores do satélite. Além disso, verificou-se que, nos trópicos, áreas menos intensas, mas mais extensas, também apresentam viés negativo e, portanto, subestimam as alturas do swell.

Dados do modelo WW3 e do satélite foram utilizados como condição inicial para o modelo SWAN, que foi utilizado em eventos em que as ondas de swell eram predominantes. Estes eventos foram selecionados com base na faixa em que o satélite (ENVISAT) mede o período da onda para uma comparação mais realista possível. No total foram selecionados 6 eventos, sendo 3 localizados na região sul e outros 3 na região nordeste entre 2002 e 2009. Para cada evento as duas simulações foram comparadas com base no tempo e espaço e também para pontos específicos localizados em águas rasas e profundas. Os resultados mostram que houve uma excelente correlação, evidenciada pelo coeficiente de Pearson, entre as duas simulações nas duas regiões estudadas, principalmente na análise espacial e temporal. Foi constatado que o *Tp*, para a simulação com dados do WW3, é subestimado em relação à simulação com dados do satélite em todos os eventos. Os resultados obtidos mostram que houve uma grande coerência entre as duas simulações. Apesar de o *Tp* apresentar disparidade maior entre as duas simulações, a tendência mostrou-se coerente tanto nos dados simulados com o WW3 como do satélite.

Este trabalho utilizou dados provenientes de satélite e de modelos numéricos de onda, onde foi comparado diversos parâmetros em escala global e regional (sul e nordeste do Brasil). Também foi comparado altura e velocidade de vento em situações de eventos extremos para a região sul do país. Os resultados mostram que ocorreu uma boa correspondência entre os dados do satélite e modelo, no entanto foi observado que os dados provenientes do satélite tendem a superestimar os dados de modelo. Uma comparação mais detalhada e com maior quantidade de dados poderia validar isto e fica como um passo a ser feito em trabalhos futuros.

7 Anexos

UNIVERSIDADE FEDERAL DO RIO GRANDE DO SUL
INSTITUTO DE GEOCIÊNCIAS
Pesquisas em Geociências

Porto Alegre, 14 de novembro de 2017.

Ao Heitor Perotto e colaboradores

Venho comunicar o recebimento do manuscrito listado, submetido para publicação em *Pesquisas em Geociências,* órgão de divulgação científica editado pelo Instituto de Geociências da Universidade Federal do Rio Grande do Sul.

Contudo, para dar prosseguimentos às atividades editoriais, é necessário realizar ajustes, necessitando, portanto, de nova submissão.

Os principais problemas encontrados dizem respeito à formatação, subdivisão do texto, incluindo a necessidade de padronizar todas as referências bibliográficas de acordo com as normas da revista, conforme poderão observar no arquivo em anexo, que deve ser utilizado para confecção de um novo arquivo e uma nova submissão.

Agradeço a seleção de *Pesquisas em Geociências* para a publicação de sua contribuição.

Observações:
a) Salvar a nova versão como o nome Man 713 Perotto et al.
b) Na mensagem eletrônica, no campo "assunto", inserir: Man 713 Perotto et al.

Manuscrito 713: Tracking extratropical cyclones which cause extreme ocean wave events in the Southwestern Atlantic Ocean.
Autores: Heitor Perotto, Leandro Farina & Elírio Ernestino Toldo Junior.

Atenciosamente,

Prof. Dr. Paulo Alves de Souza
Editor Chefe

Pesquisas em Geociências
Instituto de Geociências – Departamento de Paleontologia e Estratigrafia
Av. Bento Gonçalves, n° 9500 - Bloco 1 - Prédio 43127
CEP 91.540-000, Porto Alegre, RS, Brasil.
Email: paulo.alves.souza@ufrgs.br

Figura 7.1: Email recebimento artigo Revista Pesquisa em Geociências.

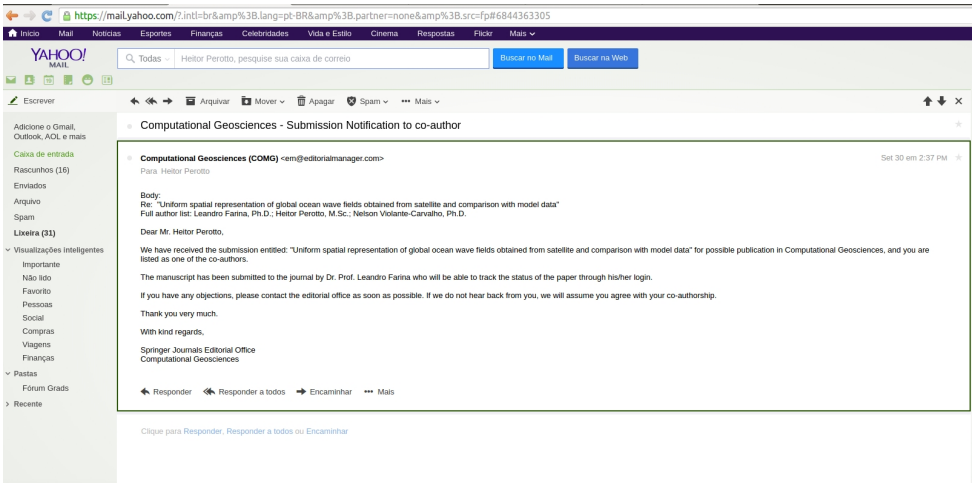

Figura 7.2: Email recebimento artigo Computational Geosciences.

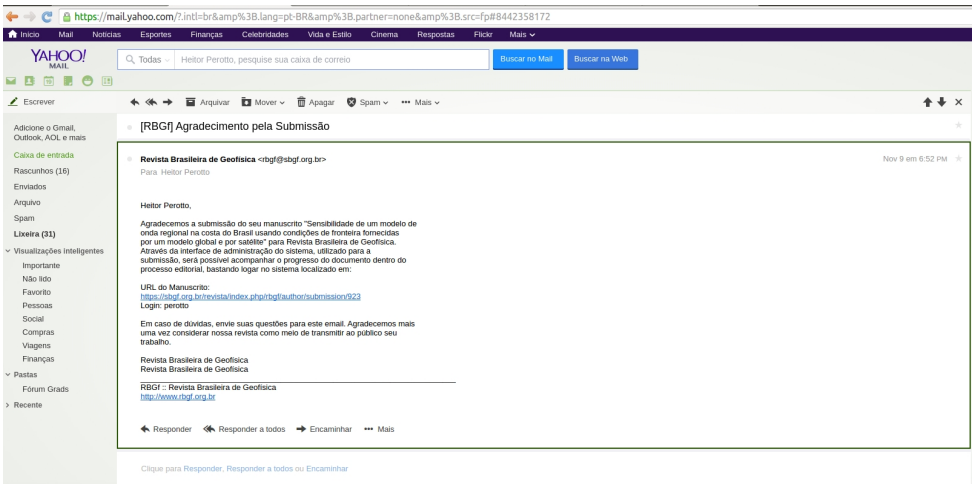

Figura 7.3: Email recebimento artigo Revista Brasileira de Geofísica.